

## Article

# An Efficient Adaptive Fuzzy Hierarchical Sliding Mode Control Strategy for 6 Degrees of Freedom Overhead Crane

Hung Van Pham <sup>1,†</sup>, Quoc-Dong Hoang <sup>2,†</sup> , Minh Van Pham <sup>1</sup>, Dung Manh Do <sup>3</sup>, Nha Hoang Phi <sup>1</sup> ,  
Duy Hoang <sup>3</sup>, Hai Xuan Le <sup>4</sup>, Thai Dinh Kim <sup>4</sup> and Linh Nguyen <sup>5,\*</sup> 

<sup>1</sup> Faculty of Electrical Engineering, Hanoi University of Industry, Hanoi 100000, Vietnam; phamvanhung@hau.edu.vn (H.V.P.); minhvp@hau.edu.vn (M.V.P.); nhaph@hau.edu.vn (N.H.P.)

<sup>2</sup> Institute of Mechanical Engineering, Vietnam Maritime University, Hai Phong 180000, Vietnam; hoangquocdong.vimaru@gmail.com

<sup>3</sup> School of Electrical Engineering, Hanoi University of Science and Technology, Hanoi 100000, Vietnam; domanh.dung180050@gmail.com (D.M.D.); duyct2304@gmail.com (D.H.)

<sup>4</sup> International School, Vietnam National University Hanoi, Hanoi 100000, Vietnam; hailx@isvnu.vn (H.X.L.); thaidk@isvnu.vn (T.D.K.)

<sup>5</sup> School of Engineering, Information Technology and Physical Sciences, Federation University Australia, Churchill, VIC 3842, Australia

\* Correspondence: l.nguyen@federation.edu.au

† These authors contributed equally to this work.

**Abstract:** The paper proposes a new approach to efficiently control a three-dimensional overhead crane with 6 degrees of freedom (DoF). Most of the works proposing a control law for a gantry crane assume that it has five output variables, including three positions of the trolley, bridge, and pulley and two swing angles of the hoisting cable. In fact, the elasticity of the hoisting cable, which causes oscillation in the cable direction, is not fully incorporated into the model yet. Therefore, our work considers that six under-actuated outputs exist in a crane system. To design an efficient controller for the 6 DoF crane, it first employs the hierarchical sliding mode control approach, which not only guarantees stability but also minimizes the sway and oscillation of the overhead crane when it transports a payload to a desired location. Moreover, the unknown and uncertain parameters of the system caused by its actuator nonlinearity and external disturbances are adaptively estimated and inferred by utilizing the fuzzy inference rule mechanism, which results in efficient operations of the crane in real time. More importantly, stabilization of the crane controlled by the proposed algorithm is theoretically proved by the use of the Lyapunov function. The proposed control approach was implemented in a synthetic environment for the extensive evaluation, where the obtained results demonstrate its effectiveness.

**Keywords:** 3D overhead crane; sliding mode control; fuzzy learning; 6 degrees of freedom



**Citation:** Pham, H.V.; Hoang, Q.-D.; Pham, M.V.; Do, D.M.; Phi, N.H.; Hoang, D.; Le, H.X.; Kim, T.D.; Nguyen, L. An Efficient Adaptive Fuzzy Hierarchical Sliding Mode Control Strategy for 6 Degrees of Freedom Overhead Crane. *Electronics* **2022**, *11*, 713. <https://doi.org/10.3390/electronics11050713>

Academic Editors: Juan M. Corchado, Stefanos Kollias and Javid Taheri

Received: 31 January 2022

Accepted: 21 February 2022

Published: 25 February 2022

**Publisher's Note:** MDPI stays neutral with regard to jurisdictional claims in published maps and institutional affiliations.



**Copyright:** © 2022 by the authors. Licensee MDPI, Basel, Switzerland. This article is an open access article distributed under the terms and conditions of the Creative Commons Attribution (CC BY) license (<https://creativecommons.org/licenses/by/4.0/>).

## 1. Introduction

Overhead crane systems have been playing a crucial role in many applications from industries or factories to transportation [1–5]. One of the typical characteristics of an overhead crane is that it is under-actuated: that is, in a crane system, the number of inputs is always smaller than the number of outputs [6]. Having more outputs than inputs, an overhead system is constrained by strong nonlinearities, internal and external uncertainties, and coupling properties. Hence, efficiently controlling an under-actuated overhead crane with fewer independent control signals than its 6 degrees of freedom is a fundamental but still challenging problem.

Due to its fundamentality, researchers, engineers, and the practitioners who design the control laws for under-actuated crane systems are always concerned with the robustness in the system response due to its parameter uncertainties and actuator nonlinearities. To

address the concern, the sliding mode control (SMC) method has been favored for those systems [7–10]. For instance, the authors in [11–13] proposed the robust SMC controllers for a gantry crane, which allow the system with uncertain parameters and nonlinear actuators to robustly work under external disturbances in a working environment. Fu et al., in the work [14], designed an adaptive sliding mode tracking controller to effectively control a dual boom crane. The proposed method was verified in a laboratory system. It is noted that the challenge in designing a robust SMC scheme for an under-actuated crane system is how to formulate sliding surfaces. In the work [15–17], the authors proposed to compute an intermediate variable from the state errors before a second-level sliding surface is formulated. In recent works [18,19], Yang et al. proposed the adaptive controllers for multi-input multi-output (MIMO) under-actuated systems given some constraints. For instance, by exploiting elaborately constructed finite-time convergent surfaces, a new control scheme in [18] can asymptotically and stably control an MIMO system under plant uncertainties and actuator deadzones. The unknown parameters of the system are trained through a fuzzy system. In the paper [19], output and velocity constraints are simultaneously considered in the control actions.

The hierarchical SMC (HSMC) approach has also been frequently utilized in defining the sliding surface for the SMC scheme in applications using under-actuated robotic systems [12,13,20,21]. For instance, Wang et al. in their works [20] defined a first-level sliding surface for each subsystem of a second-order under-actuated system. Then, they established the second-level sliding surface by simply adding the first-level sliding surfaces together.

Nonetheless, when developing an HSMC strategy for an overhead crane system, we have learned that if some parameters in the HSMC scheme are not properly chosen, it can severely cause vibration in the control system. Choosing an improper parameter for the HSMC controller is probably due to imprecision and imperfect information in the crane. This is very likely in practice, since the under-actuated crane systems are constrained by their highly complicated nonlinearities and uncertainties. So far, it is well-known that either fuzzy logic [22] or neural network [23] has been frequently exploited in addressing issues of inferring parameters for highly uncertain control systems. For instance, the fuzzy logic has been extensively employed in controlling under-actuated systems [24,25]. By exploiting the Takagi–Sugeno fuzzy model, the authors in [26] develop a closed-loop controller to automatically control the operations of a crane with 2 degrees of freedom (DoF).

Regarding the configuration of the cranes, to the best of our knowledge, most of the existing works consider a gantry system up to 5 DoF. For instance, in our previous work [1], a two-dimensional (2D) crane with two output variables including the trolley position and swing angle is considered. A three-dimensional (3D) overhead crane can have 5 DoF or output variables comprising positions of the trolley, bridge, and pulley and swing angles of the hoisting cable in  $x$  and  $y$  directions. In most of the considered crane systems, it is assumed that the hoisting cable is rigid. However, in practice, the hoisting cable can be elastic. That is, there exists oscillation of the hoisting cable in the cable direction, which constitutes a 6th output variable or degree of freedom of the 3D crane. This 6th output component is also required to be controlled, though it is under-actuated. It can now be seen that there are up to 6 DoF in one 3D overhead crane, where there are three under-actuated output variables including two swing angles and oscillation of the hoisting cable in  $x$ ,  $y$ , and the cable directions, respectively. A 3D overhead crane with 6 DoF is the object to be controlled in this study.

Therefore, we take advantages of the HSMC approach, which guarantees robustness in the control performance, to design a controller for a 3D overhead crane with 6 DoF. In the control design, it is assumed that the parameters in the HSMC law are deterministic. Nonetheless, in fact, due to the nonlinear and uncertain properties, determining those parameters in the 6 DoF crane system is impractical. Moreover, if those parameters are not properly chosen, it can lead to severe vibration in the control system. To this end, we propose to exploit the fuzzy inference rule system to adaptively infer the parameters of

the HSMC scheme over time. It is noted that the fuzzy logic can effectively estimate the parameters of a system given its imprecision and imperfect information. More importantly, the stability of the control performance in the 3D under-actuated crane obtained by the proposed approach is theoretically proved by the Lyapunov theory. Then, we extensively evaluated our algorithm in three typical scenarios in operating an overhead crane, where the obtained results are highly promising.

The remainder of the paper is arranged as follows. A model of a 3D overhead crane system with 6 DoF is introduced in Section 2. Section 3 presents how to design an HSMC law for the 6 DoF crane systems, while Section 4 discusses how to adaptively learn its parameters by the use of the fuzzy logic. The results of evaluating the proposed approach are compared and summarized in Section 5 before conclusions are drawn in Section 6. It is noted that in this work, matrices and vectors are expressed in square brackets  $[\cdot]$  or parentheses  $(\cdot)$ , while long expressions are encapsulated in braces  $\{\cdot\}$ .

### 2. A Model of 3D Overhead Crane with 6 Degrees of Freedom

Let us consider a three-dimensional (3D) overhead crane [27]. It is assumed that the trolley moves along the  $x$  direction while the bridge moves along the  $y$  direction. A pulley embedded on the trolley, as can be seen in Figure 1, plays a role of pulling a payload up and down along the  $z$  direction through a hoisting cable. Operationally, the trolley, bridge, and pulley cooperatively allow the crane to transport an object from one location to another.

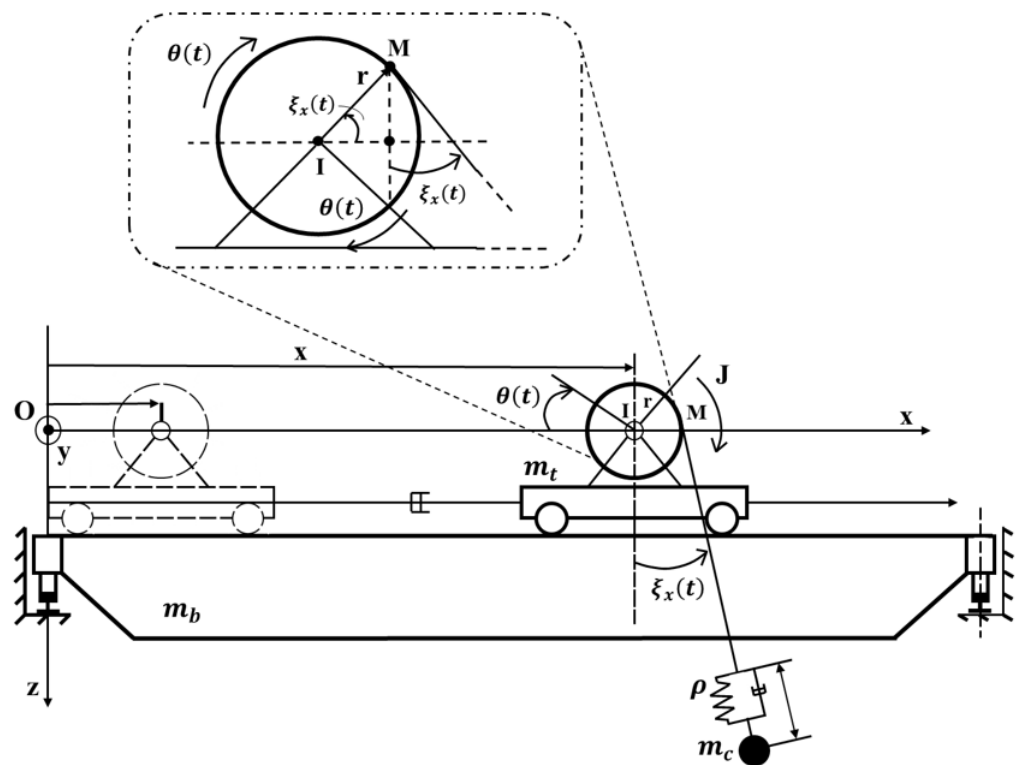


Figure 1. A digram of a 3D overhead crane model presented in the xyz plane.

Let  $x(t)$  and  $y(t)$  denote displacements of the trolley and bridge, respectively. We define  $\theta(t)$  as a rotation angle of the pulley. It is noted that under motions of the trolley, bridge, and pulley, a payload hooked to the hoisting cable swings around its equilibrium point. If we define  $O$  as the origin of a Cartesian coordinate, then the sway of the payload in the planes  $Oxz$  and  $Oyz$  is denoted by  $\xi_x(t)$  and  $\xi_y(t)$ , respectively. More importantly, in this work, we consider the elasticity of the hoisting cable. In fact, in many crane systems, the hoisting cable is not rigid but elastic. Therefore, we define  $\gamma(t)$  as the oscillation of the hoisting cable in the cable direction due to the elasticity. It can be seen that the overhead crane system has six variables, including  $x(t)$ ,  $y(t)$ ,  $\theta(t)$ ,  $\xi_x(t)$ ,  $\xi_y(t)$ , and  $\gamma(t)$ , presenting

its 6 degrees of freedom (DoF). While  $x(t)$ ,  $y(t)$ , and  $\theta(t)$  can be directly controlled by the trolley, bridge, and pulley, there is no actuator having direct connection with  $\xi_x(t)$ ,  $\xi_y(t)$ , and  $\gamma(t)$ . That is,  $\xi_x(t)$ ,  $\xi_y(t)$ , and  $\gamma(t)$  are considered as under-actuated states of the crane.

We denote  $x_d(t)$ ,  $y_d(t)$ , and  $\theta_d(t)$  as desired references of the actuated states  $x(t)$ ,  $y(t)$ , and  $\theta(t)$ , respectively, while the under-actuated states  $\xi_x(t)$ ,  $\xi_y(t)$ , and  $\gamma(t)$  are expected to reach zero during the operation of the crane. Thus,

$$\begin{aligned} \lim_{t \rightarrow +\infty} |sup(x(t))| &= x_d(t) \\ \lim_{t \rightarrow +\infty} |sup(\xi_x(t))| &= 0 \\ \lim_{t \rightarrow +\infty} |sup(y(t))| &= y_d(t) \\ \lim_{t \rightarrow +\infty} |sup(\xi_y(t))| &= 0 \\ \lim_{t \rightarrow +\infty} |sup(\theta(t))| &= \theta_d(t) \\ \lim_{t \rightarrow +\infty} |sup(\gamma(t))| &= 0 \end{aligned} \tag{1}$$

For the purpose of simplicity, we let

$$\chi(t) = [x(t)y(t) \theta(t) \xi_x(t)\xi_y(t)\gamma(t)]^T$$

denote a state vector of the 3D crane.

Apart from the hoisting cable, it is assumed that the other components in the crane are rigid, which only depend on the holonomic internal kinematic constraints. The ratio of the pulley is set to 1, while gravity  $g = 9.81 \text{ m/s}^2$ . The masses of the bridge, payload, and trolley–pulley combination are defined by  $m_b$ ,  $m_c$ , and  $m_t$ , respectively. While the elastic coefficient of the hoisting cable is defined by  $\rho$ , we denote  $J$  and  $r$  as the inertia and radius of the pulley. Hence, the potential energy of the overhead crane is computed by

$$E(t) = \left\{ \begin{aligned} &-m_c g r \cos(\xi_y(t)) \sin(\xi_x(t)) + \frac{1}{2} \rho \gamma^2 + m_c g (\gamma(t) + \Delta\gamma) \cos(\xi_x(t)) \times \\ &\times \cos(\xi_y(t)) + m_c g r (\theta(t) + \xi_x(t)) \times \cos(\xi_x(t)) \cos(\xi_y(t)) \end{aligned} \right\}. \tag{2}$$

Meanwhile, the energy loss caused by frictions is given as follows.

$$\Phi(t) = \frac{1}{2} \underline{\omega}(t)^T D \underline{\omega}(t), \tag{3}$$

where  $\underline{\omega}(t) = (\dot{\theta}(t) \ \dot{\gamma}(t) \ \dot{x}(t) \ \dot{y}(t))^T$  and  $D = \begin{pmatrix} \eta_m & 0 & 0 & 0 \\ 0 & \eta_r & 0 & 0 \\ 0 & 0 & \eta_t & 0 \\ 0 & 0 & 0 & \eta_b \end{pmatrix}$  is a matrix of the damping coefficients.

Moreover, the kinetic energy  $T(t)$  of the crane is a sum of the kinetic energy of the pulley  $T_r(t)$ , the kinetic energy of the bridge  $T_b(t)$ , the kinetic energy of the trolley  $T_t(t)$ , and the kinetic energy of the load  $T_c(t)$ .

$$T(t) = T_c(t) + T_t(t) + T_b(t) + T_r(t), \tag{4}$$

where

$$T_r(t) = \frac{1}{2} J \left( \frac{d(\theta(t))}{dt} \right)^2, \tag{5}$$

$$T_b(t) = \frac{1}{2} m_b \left( \frac{d(y(t))}{dt} \right)^2, \tag{6}$$

$$T_t(t) = \frac{1}{2}m_t \left[ \left( \frac{d}{dt}x(t) \right)^2 + \left( \frac{d}{dt}y(t) \right)^2 \right], \tag{7}$$

$$T_c(t) = \frac{1}{2}m_c \left( V_{cx}^2 + V_{cy}^2 + V_{cz}^2 \right). \tag{8}$$

It is noted that  $V_{cx}$ ,  $V_{cy}$ , and  $V_{cz}$  are velocities of the payload in the  $x$ ,  $y$ , and  $z$  directions, respectively, where they can be calculated as follows.

$$V_{cx}(t) = \left\{ \begin{array}{l} \dot{x}(t) + \dot{\gamma}(t) \sin(\xi_x(t)) + \\ + r(\dot{\theta}(t) + \dot{\xi}_x(t)) \sin(\xi_x(t)) + \\ + (\gamma(t) + \Delta\gamma)\dot{\xi}_x(t) \cos(\xi_x(t)) + \\ + (r\dot{\xi}_x(t))\dot{\xi}_x(t) \cos(\xi_x(t)) + \\ + r\theta(t)\dot{\xi}_x(t) \cos(\xi_x(t)) - \\ - r\dot{\xi}_x(t) \sin(\xi_x(t)) \end{array} \right\}. \tag{9}$$

$$V_{cy}(t) = \left\{ \begin{array}{l} \dot{y}(t) + \dot{\gamma}(t) \sin(\xi_y(t)) \cos(\xi_x(t)) + \\ + r(\dot{\theta}(t) + \dot{\xi}_x(t)) \sin(\xi_y(t)) \cos(\xi_x(t)) + \\ + (\gamma(t) + \Delta\gamma)\dot{\xi}_y(t) \cos(\xi_x(t)) \cos(\xi_y(t)) - \\ - (\gamma(t) + \Delta\gamma)\dot{\xi}_x(t) \sin(\xi_x(t)) \sin(\xi_y(t)) + \\ + r\dot{\xi}_x(t)\dot{\xi}_y(t) \cos(\xi_x(t)) \cos(\xi_y(t)) + \\ + r\theta(t) \cos(\xi_x(t)) \cos(\xi_y(t)) - \\ - r\dot{\xi}_x(t)\dot{\xi}_x(t) \sin(\xi_x(t)) \sin(\xi_y(t)) - \\ - r\theta(t)\dot{\xi}_x(t) \sin(\xi_x(t)) \sin(\xi_y(t)) \end{array} \right\}. \tag{10}$$

$$V_{cz}(t) = \left\{ \begin{array}{l} \dot{\gamma}(t)\cos(\xi_y(t)) \cos(\xi_x(t)) + \\ + r(\dot{\theta}(t) + \dot{\xi}_x(t)) \cos(\xi_y(t)) \cos(\xi_x(t)) - \\ - (\gamma(t) + \Delta\gamma)\dot{\xi}_y(t) \cos(\xi_x(t)) \sin(\xi_y(t)) - \\ - (\gamma(t) + \Delta\gamma)\dot{\xi}_x(t) \sin(\xi_x(t))\cos(\xi_y(t)) - \\ - r\dot{\xi}_x(t)\dot{\xi}_y(t) \cos(\xi_x(t)) \sin(\xi_y(t)) - \\ - r\theta(t)\dot{\xi}_y(t) \cos(\xi_x(t)) \sin(\xi_y(t)) - \\ - r\dot{\xi}_x(t)\dot{\xi}_x(t) \sin(\xi_x(t))\cos(\xi_y(t)) - \\ - r\theta(t)\dot{\xi}_x(t) \sin(\xi_x(t))\cos(\xi_y(t)) - \\ - r\dot{\xi}_x(t) \cos(\xi_y(t))\cos(\xi_x(t)) + \\ + r\dot{\xi}_y(t) \sin(\xi_x(t)) \sin(\xi_y(t)) \end{array} \right\}. \tag{11}$$

By exploiting the Euler–Lagrange equation, the crane system can be presented in the differential form as follows.

$$\frac{d}{dt} \left[ \left( \frac{\partial L(\underline{\chi}, t)}{\partial \dot{\underline{\chi}}(t)} \right) \right]^T - \left[ \frac{\partial L(\underline{\chi}, t)}{\partial \underline{\chi}(t)} \right]^T = \underline{u}(t) - \left[ \frac{\partial \Phi(\underline{\chi}, t)}{\partial \underline{\chi}(t)} \right]^T, \tag{12}$$

where

$$L = L(\underline{\chi}, t) = T(\underline{\chi}, t) - E(\underline{\chi}, t) \tag{13}$$

is the Lagrange function.

$\dot{\underline{\chi}}(t) = (\dot{x}(t) \ \dot{y}(t) \ \dot{\theta}(t) \ \dot{\xi}_x(t) \ \dot{\xi}_y(t) \ \dot{\gamma}(t))^T$  is a vector of the first-order derivative of the system states.  $\underline{u}(t) = (u_1(t) \ u_2(t) \ u_3(t) \ 0 \ 0 \ 0)^T$  is a vector of the input control signals. It is noticed that  $u_1(t)$ ,  $u_2(t)$ , and  $u_3(t)$  are the input signals to control the trolley, bridge, and pulley, respectively. The Jacobian derivatives of the Lagrange function can be computed by

$$\frac{\partial L(\underline{\chi}, t)}{\partial \underline{\chi}(t)} = \begin{bmatrix} \frac{\partial L}{\partial \dot{x}(t)} \\ \frac{\partial L}{\partial \dot{y}(t)} \\ \frac{\partial L}{\partial \dot{\theta}(t)} \\ \frac{\partial L}{\partial \dot{\xi}_x(t)} \\ \frac{\partial L}{\partial \dot{\xi}_y(t)} \\ \frac{\partial L}{\partial \dot{\gamma}(t)} \end{bmatrix}^T, \quad \frac{\partial L(\underline{\chi}, t)}{\partial \dot{\underline{\chi}}(t)} = \begin{bmatrix} \frac{\partial L}{\partial \dot{x}(t)} \\ \frac{\partial L}{\partial \dot{y}(t)} \\ \frac{\partial L}{\partial \dot{\theta}(t)} \\ \frac{\partial L}{\partial \dot{\xi}_x(t)} \\ \frac{\partial L}{\partial \dot{\xi}_y(t)} \\ \frac{\partial L}{\partial \dot{\gamma}(t)} \end{bmatrix}^T \tag{14}$$

Therefore, the dynamic model of the 3D overhead crane with 6 DoF can be represented by

$$M(\underline{\chi}, t)\ddot{\underline{\chi}} + (C(\underline{\chi}, \dot{\underline{\chi}}, t) + D)\dot{\underline{\chi}}(t) + G(\underline{\chi}, t) = \underline{u}(t), \tag{15}$$

where  $\ddot{\underline{\chi}}(t) = (\ddot{x}(t) \ \ddot{y}(t) \ \ddot{\theta}(t) \ \ddot{\xi}_x(t) \ \ddot{\xi}_y(t) \ \ddot{\gamma}(t))^T$  is a vector of the second-order derivatives of the system states.  $G(\underline{\chi}, t) = (0 \ 0 \ g_1 \ g_2 \ g_3 \ g_4)^T$  is the gravitational matrix. Calculation details of elements of  $M(\underline{\chi}, t)$ ,  $C(\underline{\chi}, \dot{\underline{\chi}}, t)$  and  $G(\underline{\chi}, t)$  can be found in Appendix A.

### 3. Hierarchical Sliding Mode Controller for 3D Overhead Crane

In this section, we will present how to design a hierarchical sliding mode control (HSMC) scheme for a 3D overhead crane with 6 DoF. It is noted that we exploit the dynamic model of the crane as introduced in Section 2.

Let us split  $\underline{\chi}(t)$  into  $\underline{\chi}(t) = (\underline{\chi}_1(t) \ \underline{\chi}_2(t))^T$ , where  $\underline{\chi}_1(t) = \begin{pmatrix} x(t) \\ y(t) \\ \theta(t) \end{pmatrix}$  is the corresponding vector of the actuated states, while  $\underline{\chi}_2(t) = \begin{pmatrix} \xi_x(t) \\ \xi_y(t) \\ \gamma(t) \end{pmatrix}$  is the corresponding vector of the under-actuated states, respectively.

$\underline{u}(t) = (\underline{\tau}(t) \ \underline{0})^T$  in which  $\underline{\tau}(t) = \begin{pmatrix} u_1(t) \\ u_2(t) \\ u_3(t) \end{pmatrix} \in \mathbb{R}^{3 \times 1}$ . We now define  $K(\underline{\chi}, t) = M^{-1}(\underline{\chi}, t) = \begin{pmatrix} K_1(\underline{\chi}, t) & K_3(\underline{\chi}, t) \\ K_2(\underline{\chi}, t) & K_4(\underline{\chi}, t) \end{pmatrix}$  with  $K_1(\underline{\chi}, t)$ ,  $K_2(\underline{\chi}, t)$ ,  $K_3(\underline{\chi}, t)$  and  $K_4(\underline{\chi}, t) \in \mathbb{R}^{3 \times 3}$ . And  $C(\underline{\chi}, \dot{\underline{\chi}}, t) = \begin{pmatrix} C_1(\underline{\chi}, \dot{\underline{\chi}}, t) & C_3(\underline{\chi}, \dot{\underline{\chi}}, t) \\ C_2(\underline{\chi}, \dot{\underline{\chi}}, t) & C_4(\underline{\chi}, \dot{\underline{\chi}}, t) \end{pmatrix}$  with  $C_1(\underline{\chi}, \dot{\underline{\chi}}, t)$ ,  $C_2(\underline{\chi}, \dot{\underline{\chi}}, t)$ ,  $C_3(\underline{\chi}, \dot{\underline{\chi}}, t)$ , and  $C_4(\underline{\chi}, \dot{\underline{\chi}}, t) \in \mathbb{R}^{3 \times 3}$ .

Moreover,

$$G(\underline{\chi}, t) = \begin{pmatrix} G_1(\underline{\chi}, t) \\ G_2(\underline{\chi}, t) \end{pmatrix},$$

where

$$G_1(\underline{\chi}, t) = \begin{pmatrix} 0 \\ 0 \\ g_1 \end{pmatrix}, \quad G_2(\underline{\chi}, t) = \begin{pmatrix} g_2 \\ g_3 \\ g_4 \end{pmatrix}.$$

Therefore,

$$\dot{\underline{\chi}}_1(t) = \underline{f}_1(\underline{\chi}, \dot{\underline{\chi}}, t) + K_1(\underline{\chi}, t)\underline{\tau} \tag{16}$$

$$\dot{\underline{\chi}}_2(t) = \underline{f}_2(\underline{\chi}, \dot{\underline{\chi}}, t) + K_2(\underline{\chi}, t)\underline{\tau} \tag{17}$$

where

$$\underline{f}_1(\underline{\chi}, \dot{\underline{\chi}}, t) = - \left\{ \begin{array}{l} (K_1(\underline{\chi}, t)G_1(\underline{\chi}, t) + \\ + K_3(\underline{\chi}, t)G_2(\underline{\chi}, t)) + \\ + K_1(\underline{\chi}, t)C_1(\underline{\chi}, \dot{\underline{\chi}}, t)\dot{\underline{\chi}}_1(t) + \\ + K_3(\underline{\chi}, t)C_2(\underline{\chi}, \dot{\underline{\chi}}, t)\dot{\underline{\chi}}_1(t) + \\ + K_1(\underline{\chi}, t)C_3(\underline{\chi}, \dot{\underline{\chi}}, t)\dot{\underline{\chi}}_2(t) + \\ + K_3(\underline{\chi}, t)C_4(\underline{\chi}, \dot{\underline{\chi}}, t)\dot{\underline{\chi}}_2(t) \end{array} \right\}, \tag{18}$$

$$\underline{f}_2(\underline{\chi}, \dot{\underline{\chi}}, t) = - \left\{ \begin{array}{l} (K_2(\underline{\chi}, t)G_1(\underline{\chi}, t) + \\ + K_4(\underline{\chi}, t)G_2(\underline{\chi}, t)) + \\ + K_2(\underline{\chi}, t)C_1(\underline{\chi}, \dot{\underline{\chi}}, t)\dot{\underline{\chi}}_1(t) + \\ + K_4(\underline{\chi}, t)C_2(\underline{\chi}, \dot{\underline{\chi}}, t)\dot{\underline{\chi}}_1(t) + \\ + K_2(\underline{\chi}, t)C_3(\underline{\chi}, \dot{\underline{\chi}}, t)\dot{\underline{\chi}}_2(t) + \\ + K_4(\underline{\chi}, t)C_4(\underline{\chi}, \dot{\underline{\chi}}, t)\dot{\underline{\chi}}_2(t) \end{array} \right\}. \tag{19}$$

The model in (16) and (17) can be represented as a state model by

$$\dot{\underline{x}}_1(t) = \underline{x}_2(t), \tag{20}$$

$$\dot{\underline{x}}_2(t) = \underline{f}_1(\underline{\chi}, \dot{\underline{\chi}}, t) + K_1(\underline{\chi}, t)\underline{\tau}, \tag{21}$$

$$\dot{\underline{x}}_3(t) = \underline{x}_4(t), \tag{22}$$

$$\dot{\underline{x}}_4(t) = \underline{f}_2(\underline{\chi}, \dot{\underline{\chi}}, t) + K_2(\underline{\chi}, t)\underline{\tau}, \tag{23}$$

where  $\underline{x}_1 = \underline{\chi}_1$ ,  $\underline{x}_2 = \dot{\underline{\chi}}_1$ ,  $\underline{x}_3 = \underline{\chi}_2$  and  $\underline{x}_4 = \dot{\underline{\chi}}_2$ . Let

$$\underline{e}_1(t) = \underline{x}_1(t) - \underline{x}_{1d}(t)$$

$$\underline{e}_3(t) = \underline{x}_3(t) - \underline{x}_{3d}(t)$$

denote errors between the output signals ( $\underline{x}_1(t)$ ,  $\underline{x}_3(t)$ ) and the desired references ( $\underline{x}_{1d}(t)$ ,  $\underline{x}_{3d}(t)$ ).  $\underline{x}_{1d}(t) = \begin{pmatrix} x_d \\ y_d \\ \theta_d \end{pmatrix}$  is a vector of the desired references of the actuated states while

$\underline{x}_{3d}(t) = \begin{pmatrix} 0 \\ 0 \\ 0 \end{pmatrix}$  is a vector of the desired references of the under-actuated states. The errors can now be specified by

$$\dot{\underline{e}}_1(t) = \underline{e}_2(t), \tag{24}$$

$$\dot{\underline{e}}_2(t) = \underline{f}_1(\underline{\chi}, \dot{\underline{\chi}}, t) + K_1(\underline{\chi}, t)\underline{\tau} - \dot{\underline{x}}_{1d}(t), \tag{25}$$

$$\dot{\underline{e}}_3(t) = \underline{e}_4(t), \tag{26}$$

$$\dot{e}_4(t) = \underline{f}_2(\underline{\chi}, \dot{\underline{\chi}}, t) + K_2(\underline{\chi}, t) \cdot \underline{\tau} \tag{27}$$

In order to minimize the errors in (24)–(27), the control strategy is proposed as follows.

$$\underline{\tau}(t) = \left\{ \underline{\tau}_{1eq}(t) + \underline{\tau}_{2eq}(t) - \left( \lambda_1 K_1(\underline{\chi}, t) + \lambda_2 K_2(\underline{\chi}, t) \right)^{-1} \times \left\{ \begin{array}{l} \lambda_1 K_1(\underline{\chi}, t) \underline{\tau}_{2eq}(t) + \\ + \lambda_2 K_2(\underline{\chi}, t) \underline{\tau}_{1eq}(t) + \\ + \eta_3 \underline{s}(t) + \eta_4 \text{sign}(\underline{s}(t)) \end{array} \right\} \right\} \tag{28}$$

where  $\lambda_1, \lambda_2, \alpha_1, \alpha_2 \in \mathbb{R}^{3 \times 3}$  are the symmetric, positive-definite, and constant matrices, while  $\eta_3$  and  $\eta_4$  are the symmetric and positive-definite matrices. The second-level sliding surface is compiled by two first-level sliding surfaces from two subsystems as follows.

$$\underline{s}(t) = \lambda_1 \underline{s}_1(t) + \lambda_2 \underline{s}_2(t),$$

where

$$\underline{s}_1(t) = \alpha_1 \underline{e}_1(t) + \underline{e}_2(t). \tag{29}$$

$$\underline{s}_2(t) = \alpha_2 \underline{e}_3(t) + \underline{e}_4(t). \tag{30}$$

Thus, two control signals for two subsystems are given by

$$\underline{\tau}_{1eq} = -K_1^{-1}(\underline{\chi}, t) \left( \alpha_1 \underline{e}_2(t) + \underline{f}_1(\underline{\chi}, \dot{\underline{\chi}}, t) - \ddot{\underline{x}}_{1d}(t) \right), \tag{31}$$

$$\underline{\tau}_{2eq} = -K_2^{-1}(\underline{\chi}, t) \left( \alpha_2 \underline{e}_4(t) + \underline{f}_2(\underline{\chi}, \dot{\underline{\chi}}, t) \right). \tag{32}$$

The stability of the proposed control law can be specified by the following lemma.

**Lemma 1.** *The proposed control scheme (28) guarantees stability of the 3D overhead crane with 6 DoF, which leads to  $\lim_{t \rightarrow +\infty} \underline{e}_j(t) = \underline{0}, j = 1, \dots, 4$ .*

**Proof.** Let us consider the first subsystem represented by

$$\dot{\underline{x}}_1(t) = \underline{x}_2(t), \tag{33}$$

$$\dot{\underline{x}}_2(t) = \underline{f}_1(\underline{\chi}, \dot{\underline{\chi}}, t) + K_1(\underline{\chi}, t) \underline{\tau}_1, \tag{34}$$

where its sliding surface is

$$\underline{s}_1(t) = \alpha_1 \underline{e}_1(t) + \underline{e}_2(t). \tag{35}$$

To obtain  $\lim_{t \rightarrow +\infty} \underline{s}_1(t) = \underline{0}$ , we consider the Lyapunov function candidate of  $\underline{s}_1(t)$  as follows.

$$\underline{V}_1(\underline{s}_1(t)) = \frac{1}{2} \underline{s}_1^T(t) \underline{s}_1(t). \tag{36}$$

Taking the derivative of both sides of Equation (30) yields

$$\dot{\underline{V}}_1(t) = \underline{s}_1^T(t) \dot{\underline{s}}_1(t) = \underline{s}_1^T(t) \left( \alpha_1 \underline{e}_2(t) + \underline{f}_1(\underline{\chi}, \dot{\underline{\chi}}, t) + K_1(\underline{\chi}, t) \underline{\tau}_1 - \ddot{\underline{x}}_{1d}(t) \right)$$

The control signal for the first subsystem includes the equivalent control law  $\underline{\tau}_{1eq}(t)$  and the switch control scheme  $\underline{\tau}_{1sw}(t)$ . Hence,

$$\underline{V}_1(t) = \underline{s}_1^T(t) \left\{ \begin{array}{l} \alpha_1 \underline{e}_2(t) + \underline{f}_1(\underline{\chi}, \dot{\underline{\chi}}, t) + \\ + K_1(\underline{\chi}, t) \left( \underline{\tau}_{1eq} + \underline{\tau}_{1sw} \right) - \\ - \ddot{\underline{x}}_{1d}(t) \end{array} \right\}.$$

That is,

$$\underline{V}_1(t) = \underline{s}_1^T(t) \times \left\{ \begin{array}{l} \alpha_1 \underline{e}_2(t) + \underline{f}_1(\underline{\chi}, \dot{\underline{\chi}}, t) + K_1(\underline{\chi}, t) \underline{\tau}_{1eq} - \dot{\underline{x}}_{1d}(t) + \\ + K_1(\underline{\chi}, t) \underline{\tau}_{1sw} + \eta_1 \underline{s}_1(t) + \eta_2 \text{sign}(\underline{s}_1(t)) - \\ - \eta_1 \underline{s}_1(t) - \eta_2 \text{sign}(\underline{s}_1(t)) \end{array} \right\}, \tag{37}$$

where  $\eta_1$  and  $\eta_2$  are the symmetric and positive-definite matrices. If

$$\left\{ \begin{array}{l} K_1(\underline{\chi}, t) \underline{\tau}_{1eq} + \alpha_1 \underline{e}_2(t) + \underline{f}_1(\underline{\chi}, \dot{\underline{\chi}}, t) - \dot{\underline{x}}_{1d}(t) = \underline{0}, \\ K_1(\underline{\chi}, t) \underline{\tau}_{1sw}(t) + \eta_1 \underline{s}_1(t) + \eta_2 \text{sign}(\underline{s}_1(t)) = \underline{0}, \end{array} \right. \tag{38}$$

then one has

$$\dot{\underline{V}}_1(t) = -\underline{s}_1^T(t) \eta_1 \underline{s}_1(t) - \underline{s}_1^T(t) \eta_2 \text{sign}(\underline{s}_1(t)) \leq 0,$$

which guarantees stability of the first subsystem.

Likewise, the second subsystem

$$\dot{\underline{e}}_3(t) = \underline{e}_4(t), \tag{39}$$

$$\dot{\underline{e}}_4(t) = \underline{f}_2(\underline{\chi}, \dot{\underline{\chi}}, t) + K_2(\underline{\chi}, t) \underline{\tau}_2, \tag{40}$$

where its sliding surface is

$$\underline{s}_2(t) = \alpha_3 \underline{e}_3(t) + \underline{e}_4(t), \tag{41}$$

also holds

$$K_2(\underline{\chi}, t) \underline{\tau}_{2eq} + \alpha_2 \underline{e}_4(t) + \underline{f}_2(\underline{\chi}, \dot{\underline{\chi}}, t) = \underline{0}. \tag{42}$$

Now, considering the whole crane system, given the condition  $\lim_{t \rightarrow +\infty} \underline{s}(t) = 0$  of the second-level sliding surface

$$\underline{s}(t) = \lambda_1 \underline{s}_1(t) + \lambda_2 \underline{s}_2(t), \tag{43}$$

the Lyapunov function candidate can be presented by

$$\underline{V}(\underline{s}(t)) = \frac{1}{2} \underline{s}^T(t) \underline{s}(t). \tag{44}$$

In other words,

$$\dot{\underline{V}}(t) = \underline{s}^T(t) (\lambda_1 \dot{\underline{s}}_1(t) + \lambda_2 \dot{\underline{s}}_2(t)) = \underline{s}^T(t) \left\{ \begin{array}{l} \lambda_1 \left\{ \begin{array}{l} \alpha_1 \underline{e}_2(t) + \underline{f}_1(\underline{\chi}, \dot{\underline{\chi}}, t) + \\ + K_1(\underline{\chi}, t) \underline{\tau} - \dot{\underline{x}}_{1d}(t) + \end{array} \right\} \\ + \lambda_2 \left( \alpha_2 \underline{e}_4(t) + \underline{f}_2(\underline{\chi}, \dot{\underline{\chi}}, t) + K_2(\underline{\chi}, t) \underline{\tau} \right) \end{array} \right\}. \tag{45}$$

If the control signal of the second subsystem is also presented by two components of  $\tau_{1eq}(t)$  and  $\tau_{1sw}(t)$ , then

$$\dot{\underline{V}}(t) = \underline{s}^T(t) \left\{ \begin{array}{l} \lambda_1 \left\{ \begin{array}{l} \alpha_1 e_2(t) + \underline{f}_1(\underline{\chi}, \dot{\underline{\chi}}, t) - \\ - \ddot{\underline{x}}_{1d}(t) + K_1(\underline{\chi}, t) \tau_{1eq}(t) + \\ + K_1(\underline{\chi}, t) \times \\ \times \left\{ \begin{array}{l} \tau_{1sw}(t) + \tau_{2sw}(t) + \\ + \tau_{2eq}(t) \end{array} \right\} \end{array} \right\} + \\ + \lambda_2 \left\{ \begin{array}{l} \alpha_2 e_4(t) + \underline{f}_2(\underline{\chi}, \dot{\underline{\chi}}, t) + \\ + K_2(\underline{\chi}, t) \tau_{2eq}(t) + \\ + K_2(\underline{\chi}, t) \times \\ \times \left\{ \begin{array}{l} \tau_{1sw}(t) + \tau_{2sw}(t) + \\ + \tau_{1eq}(t) \end{array} \right\} \end{array} \right\} \end{array} \right\}.$$

Therefore, the control signal for the 3D overhead crane can be specified by

$$\underline{\tau} = \tau_{1eq}(t) + \tau_{1sw}(t) + \tau_{2eq}(t) + \tau_{2sw}(t). \tag{46}$$

If one chooses

$$\left\{ \begin{array}{l} \left( \lambda_1 K_1(\underline{\chi}, t) + \lambda_2 K_2(\underline{\chi}, t) \right) \times \\ \times \left( \tau_{1sw}(t) + \tau_{2sw}(t) \right) \\ + \lambda_1 K_1(\underline{\chi}, t) \tau_{2eq}(t) + \\ + \lambda_2 K_2(\underline{\chi}, t) \tau_{1eq}(t) + \\ + \eta_3 \underline{s}(t) + \eta_4 \text{sign}(\underline{s}(t)) \end{array} \right\} = 0,$$

which leads to

$$\tau_{1sw}(t) + \tau_{2sw}(t) = \left\{ \begin{array}{l} - \left( \lambda_1 K_1(\underline{\chi}, t) + \lambda_2 K_2(\underline{\chi}, t) \right)^{-1} \times \\ \left\{ \begin{array}{l} \lambda_1 K_1(\underline{\chi}, t) \tau_{2eq}(t) \\ + \lambda_2 K_2(\underline{\chi}, t) \tau_{1eq}(t) \\ + \eta_3 \underline{s}(t) + \eta_4 \text{sign}(\underline{s}(t)) \end{array} \right\} \end{array} \right\}, \tag{47}$$

then it has

$$\tau_{1sw}(t) + \tau_{2sw}(t) = \left\{ \begin{array}{l} - \left( \lambda_1 K_1(\underline{\chi}, t) + \lambda_2 K_2(\underline{\chi}, t) \right)^{-1} \times \\ \left\{ \begin{array}{l} \lambda_1 K_1(\underline{\chi}, t) \tau_{2eq}(t) + \\ + \lambda_2 K_2(\underline{\chi}, t) \tau_{1eq}(t) + \\ + \eta_3 \underline{s}(t) + \eta_4 \text{sign}(\underline{s}(t)) \end{array} \right\} \end{array} \right\}.$$

In other words, substituting (47) into (46) completes the proof.  $\square$

It is noted that in the proposed control law (28), the phenomenon of oscillation on the sliding surface may appear due to the change in  $\text{sign}(\underline{s}(t))$ . To mitigate the issue, it is

proposed to utilize the function  $sat(\underline{s}(t))$  rather than  $sign(\underline{s}(t))$ . The function  $sat(\underline{s}(t))$  is specified by

$$sat(\underline{s}(t)) = \begin{cases} sign(\underline{s}(t)) & \text{if } |\underline{s}(t)| \geq 1 \\ \underline{s}(t) & \text{if } |\underline{s}(t)| < 1. \end{cases}$$

#### 4. Adaptive Fuzzy Learning Scheme

It can be seen in the analysis of Section 3 that if the parameters  $\alpha_1, \alpha_2, \lambda_1,$  and  $\lambda_2$  of the control strategy in (28) are fixed, it causes vibration in the sliding mode control system. In order to address the issue, in this work, we propose to adaptively learn these parameters over time by the use of a fuzzy system. To simplify the learning process, it is proposed to learn  $\alpha_1$  only. The other parameters are adapted through  $\alpha_1$  accordingly as follows.

$$\alpha_2 = A_2.\alpha_1, \lambda_1 = A_3.\alpha_1, \lambda_2 = A_4.\alpha_1,$$

where  $A_i$  is a predefined diagonal positive matrix. It is noted that varying  $A_i$  leads to a change of the sliding surfaces. If  $A_i$  is properly chosen, the control system states move on the sliding surfaces to converge to zero, which effectively minimizes the chattering phenomena in the under-actuated crane systems.

We now investigate how to learn the matrix  $\alpha_1$ . Let us assume  $\alpha_1$  has the following form.

$$\alpha_1 = \begin{bmatrix} a & 0 & 0 \\ 0 & b & 0 \\ 0 & 0 & c \end{bmatrix},$$

where  $a, b,$  and  $c$  are the parameters that will be adaptively learned by using the fuzzy inference rule system.

The parameters  $a, b,$  and  $c$  are learned through a fuzzy logic system given the input language variables  $e_x = x - x_d$  and  $\dot{e}_x, e_y = y - y_d$  and  $\dot{e}_y, e_\theta = \theta - \theta_d$  and  $\dot{e}_\theta,$  respectively. It is noted that each input language variable consists of a three-triangular fuzzy set  $[-1 \ 0 \ 1]$ . The continuous functions of the input language variables are shown in Figure 2. By using the Sugeno model, the output variables are presented by  $[-2 \ -1 \ 0 \ 1 \ 2]$ , which corresponds to  $[a_1 \ a_2 \ a_3 \ a_4 \ a_5] = [0.2 \ 0.4 \ 0.6 \ 0.4 \ 0.2]$  for learning  $a,$   $[b_1 \ b_2 \ b_3 \ b_4 \ b_5] = [0.1 \ 0.3 \ 0.5 \ 0.1 \ 0.1]$  for learning  $b,$  and  $[c_1 \ c_2 \ c_3 \ c_4 \ c_5] = [15 \ 10 \ 5 \ 10 \ 15]$  for learning  $c.$

The fuzzy inference rule system is shown in Table 1. The table is designed based on the error  $e$  and its derivative  $\dot{e}$ . Given the output variables, there are nine possible outputs in Table 1. For instance, when  $e = 1$  and  $\dot{e} = 1,$  the error in the control signal is positive and increasing. That is, reducing and negating  $\dot{e}$  are required. This can be done by setting the output of the fuzzy logic system to the variable  $-2$ . However, when  $e = 1$  and  $\dot{e} = 0,$  although the error in the control signal is positive, it is not increasing. In that case, only reducing  $\dot{e}$  is required by setting the output of the fuzzy logic system to the variable  $-1$ . In a perfect scenario when  $e = 0$  and  $\dot{e} = 0,$  no control is required, and the output of the fuzzy logic system is set to the variable 0.

**Table 1.** The inference fuzzy system for learning  $a, b,$  and  $c.$

Parameter ( $a, b, c$ )		-1	$e_i$ 0	1
$e_i$	-1	2	1	0
	0	1	0	-1
	1	0	-1	-2

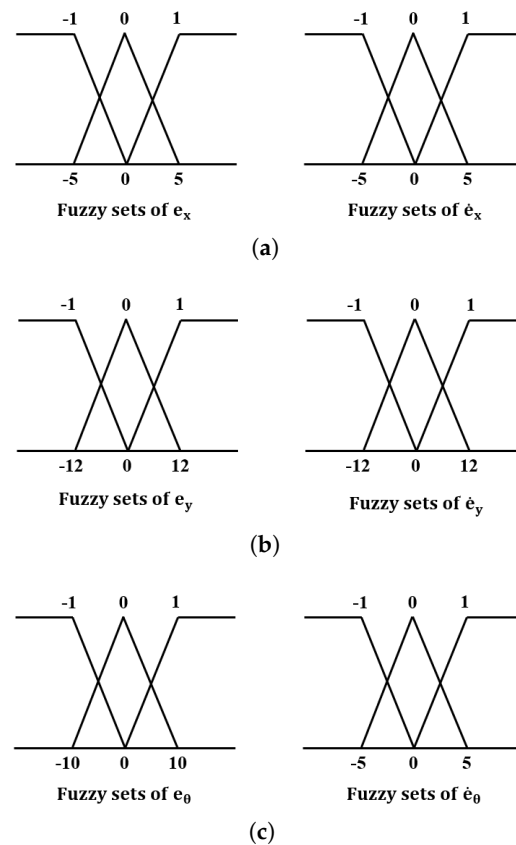


**Figure 2.** The fuzzy sets of the input language variables. (a) Learning  $a$  given  $e_x$  and  $\dot{e}_x$ . (b) Learning  $b$  given  $e_y$  and  $\dot{e}_y$ . (c) Learning  $c$  given  $\theta$  and  $\dot{\theta}$ .

Therefore, the structure of the hierarchical sliding mode control system for the 3D overhead crane given the adaptive fuzzy learning scheme is now depicted in Figure 3.

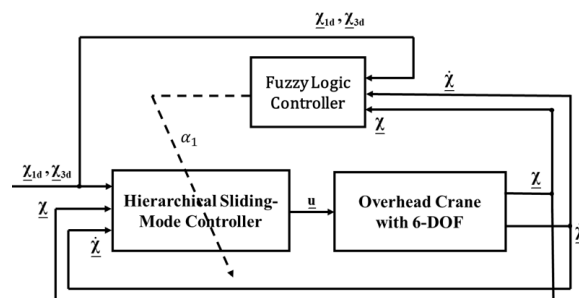


**Figure 3.** Control structure of adaptive fuzzy system.

### 5. Results and Discussions

In order to demonstrate effectiveness of our proposed approach, the adaptive fuzzy hierarchical sliding mode controller (FuzzyHSMC), in controlling the 3D overhead crane with 6 DoF, we conducted the experiments in the synthetic simulation environment. The obtained results are presented in this section. It is noticed that the control performance is measured by how effectively the crane can move to a desired location given the proposed control algorithm. In other words, it is expected that the positions of the trolley, bridge, and pulley can reach the reference values while the swing angles of the hoisting cable around a vertical line as well as the oscillation of the hoisting cable in the cable direction due to the elasticity are minimized in a reasonable time frame.

It is noted that in the experiments, the overhead crane was expected to transport a heavy payload of 500 kg. The parameters of the crane system are summarized in Table 2.

The parameters of the controllers are also encapsulated in Table 3. For comparison purposes, there were two controllers including HSMC, as presented in Section 3 and the proposed FuzzyHSMC implemented in the experiments. It is noticed that the HSMC is a deterministic control scheme where all the parameters of the controller are required to be known. However, in practice, the control parameters are unknown and uncertain, which makes the HSMC impractical. In our proposed control approach, the parameters of the FuzzyHSMC are adaptively learned over time by the use of the inference fuzzy system, as presented in Section 4. The learning scheme allows the proposed controller to well adapt to the nonlinearity and uncertainty of the real-world crane systems.

**Table 2.** The parameters of the 3D overhead crane.

Parameter	Value	Unit
$m_b$	2316.5	kg
$m_c$	500	kg
$m_t$	371.9	kg
J	180	kg·m <sup>2</sup>
r	0.31	m
g	9.81	m/s <sup>2</sup>
$\rho$	300,000	N/m
$\Delta\gamma$	0.01	m
$\eta_b$	350	N·m/s
$\eta_t$	310	N·m/s
$\eta_m$	170	N·m/s
$\eta_r$	260	N·m/s

**Table 3.** The parameters of the controllers.

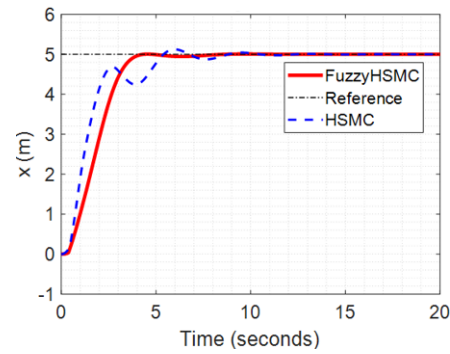
Parameter	Value
$\lambda_1$	diag([0.6 0.5 4])
$\lambda_2$	diag([1.2 1.5 1])
$\alpha_1$	diag([0.6 0.2 1.3])
$\alpha_2$	diag([2.4 0.7 0.8])
$\eta_3$	diag([0.2 1.6 0.1])
$\eta_4$	diag([4 1.6 0.6])
$A_2$	diag([3 5 0.05])
$A_3$	diag([1 0.5 0.1])
$A_4$	diag([5 1.6 0.15])

To demonstrate that the proposed approach can efficiently control a 3D overhead crane with 6 DoF in a variety of scenarios, we conducted three typical experiments. In the first, the reference levels were set to be constant, while in the second, the desired positions of the trolley, bridge, and pulley were changed during the crane's operation. In the third scenario, we considered the influence of external disturbances on the control quality of the crane system and how the proposed control law could address the disturbance issues.

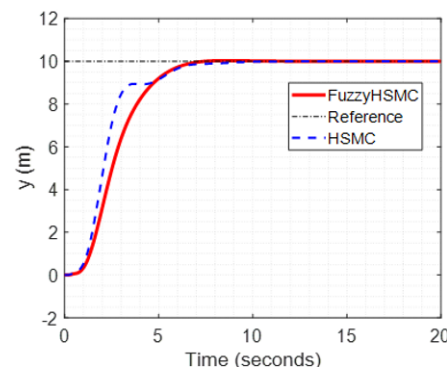
### 5.1. Constant Input

In the first scenario, it was expected for the overhead crane to transport the 500 kg payload from an initial position [0 0 0 0 0] to a desired location where the final positions for the trolley, bridge, and pulley are  $x_d = 5$  m,  $y_d = 10$  m, and  $\theta_d = 5$  rad, respectively. The results obtained by two control algorithms, HSMC and FuzzyHSMC, on the control performances of six controlled variables including  $x(t)$ ,  $y(t)$ ,  $\theta(t)$ ,  $\zeta_x(t)$ ,  $\zeta_y(t)$ , and  $\gamma(t)$  are depicted in Figures 4 and 5. It can be seen that all the controlled variables could reach 95% of the reference levels within approximately 6 s. More importantly, there is no overshoot in the actuated states while the overshoots in the under-actuated states are relatively small. Under our proposed approach, the overshoots of the sway angles are smaller than 0.1 and

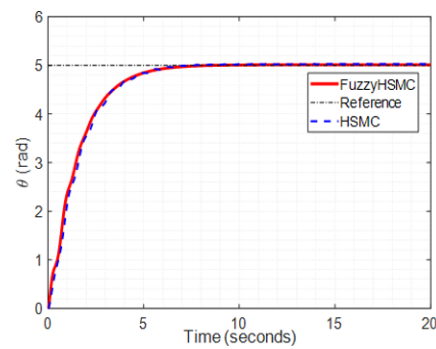
0.3 degrees for  $\zeta_x(t)$  and  $\zeta_y(t)$ , respectively, while the oscillation of the hoisting cable is less than 0.2 cm. Overall, while the results obtained by both the controllers in the actuated states are comparable, the proposed control law FuzzyHSMC outperforms the HSMC in the under-actuated components, as can be seen in Figure 5.



(a)



(b)



(c)

**Figure 4.** The actuated states given the constant input. (a) The trolley position  $x(t)$ . (b) The bridge position  $y(t)$ . (c) The pulley angle  $\theta(t)$ .

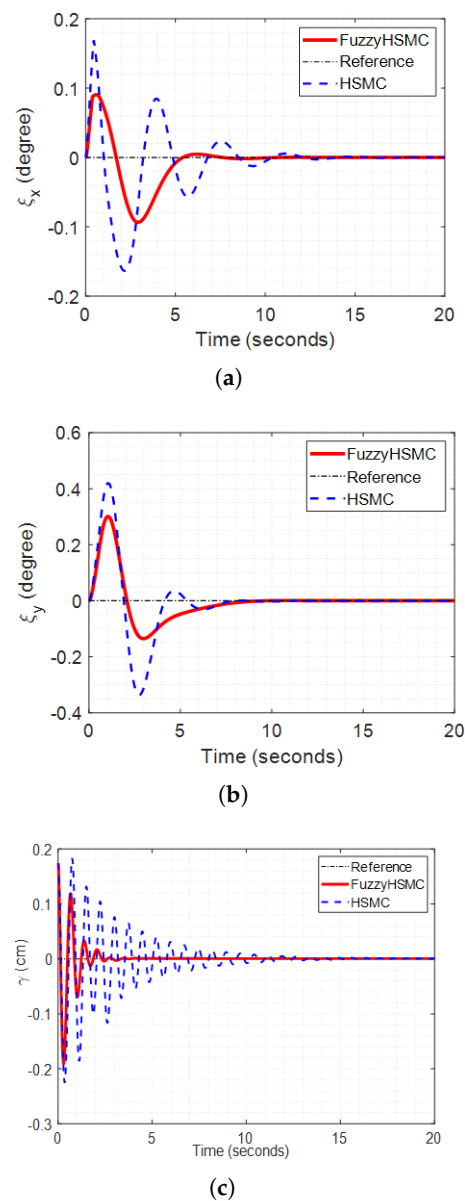
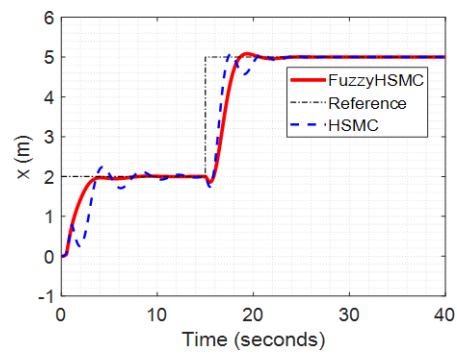


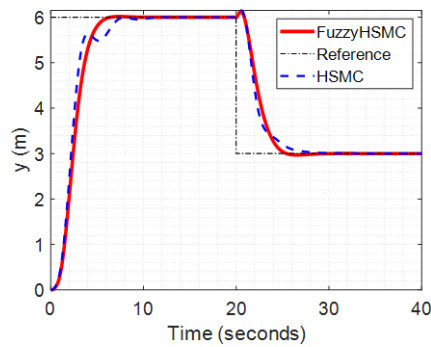
**Figure 5.** The under-actuated states given the constant input. (a) The sway of the payload in  $Oxz$ ,  $\xi_x(t)$ . (b) The sway of the payload in  $Oyz$ ,  $\xi_y(t)$ . (c) The oscillation of the hoisting cable in the cable direction,  $\gamma(t)$ .

### 5.2. Step Input

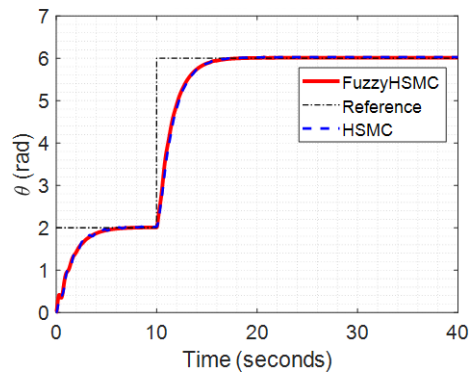
In the second scenario, the desired positions of the trolley, bridge, and pulley were first set to  $x_d = 2$  m,  $y_d = 6$  m, and  $\theta_d = 2$  rad, respectively. Nonetheless, at 10 s from the beginning, the final position of the pulley was then set to  $\theta_d = 6$  rad. Likewise, at 15 s, the final position of the trolley was set to  $x_d = 5$  m, and at 20 s, the final position of the bridge was set back to  $y_d = 3$  m. Although there were changes of the reference levels during the operation of the crane, the control algorithms adapted very well in efficiently controlling the motions of the trolley, bridge, and pulley, as demonstrated in Figure 6. Moreover, the changes in the control inputs are also reflected in the responses of the under-actuated components, as illustrated in Figure 7. For instance, although the sway angles and oscillation of the hoisting cable were suppressed almost to zero after about 6 s, they re-emerged at the time there were the changes in the control inputs. However, the maximum amplitudes of these unexpected swings and oscillation are minor at about 0.1 degrees with respect to  $\xi_x(t)$  and  $\xi_y(t)$  and 0.05 cm with respect to  $\gamma(t)$ . Then, the under-actuated states went down to zero again after a few seconds, as can be seen in Figure 7.



(a)

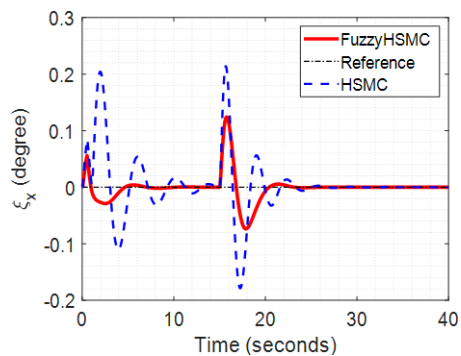


(b)



(c)

**Figure 6.** The actuated states given the step input. (a) The trolley position  $x(t)$ . (b) The bridge position  $y(t)$ . (c) The pulley angle  $\theta(t)$ .



(a)

**Figure 7.** Cont.

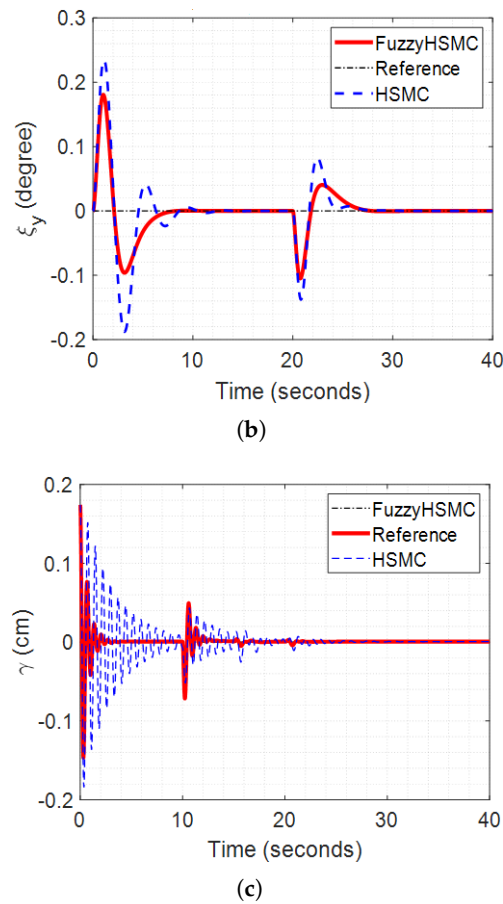


**Figure 7.** The under-actuated states given the step input. (a) The sway of the payload in  $Oxz$ ,  $\xi_x(t)$ . (b) The sway of the payload in  $Oyz$ ,  $\xi_y(t)$ . (c) The oscillation of the hoisting cable in the cable direction,  $\gamma(t)$ .

### 5.3. Noisy Input

In fact, there are always external disturbances influencing the operations of the real-world crane systems. Hence, in the third experiment, we simulated the external disturbances in the form of pulses injecting into the crane at different times. For instance, at 10 s from the beginning, a 2 s width pulse with an amplitude of  $-500 \text{ N}\cdot\text{m}$  considered as a noise was injected into the pulley. In a similar fashion, at 15 and 25 s, two 5 s width pulses with amplitudes of 1000 N and 2000 N were injected into the trolley and bridge, respectively. The external disturbances are depicted in Figure 8.

It is noted that in this third experiment, the final positions of the trolley, bridge, and pulley were also set to  $x_d = 5 \text{ m}$ ,  $y_d = 10 \text{ m}$ , and  $\theta_d = 5 \text{ rad}$ . The obtained results presenting the control performances are illustrated in Figures 9 and 10. Undoubtedly, it can be seen that the external disturbances caused deterioration of the control performances at the time the disturbances were injected into the crane. However, the controllers quickly steered both the actuated and under-actuated states back to the desired positions. More importantly, as can be seen in Figure 10, given our control technique, the influence caused by the external disturbances on the under-actuated components is insignificant.

Given the results in all three scenarios, it can be seen that since the proposed control algorithm FuzzyHSMC can adaptively learn its parameters over time, it outperforms the deterministic control scheme HSMC.

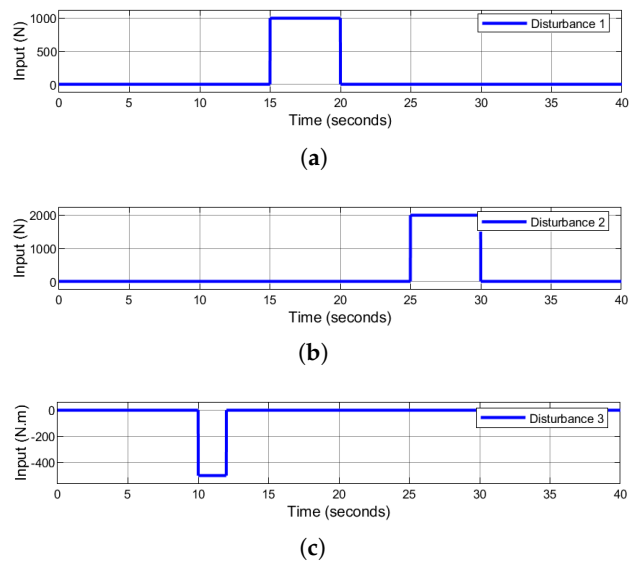


**Figure 8.** The external disturbances to the crane system. (a) The external disturbance on the trolley. (b) The external disturbance on the bridge. (c) The external disturbance on the pulley.

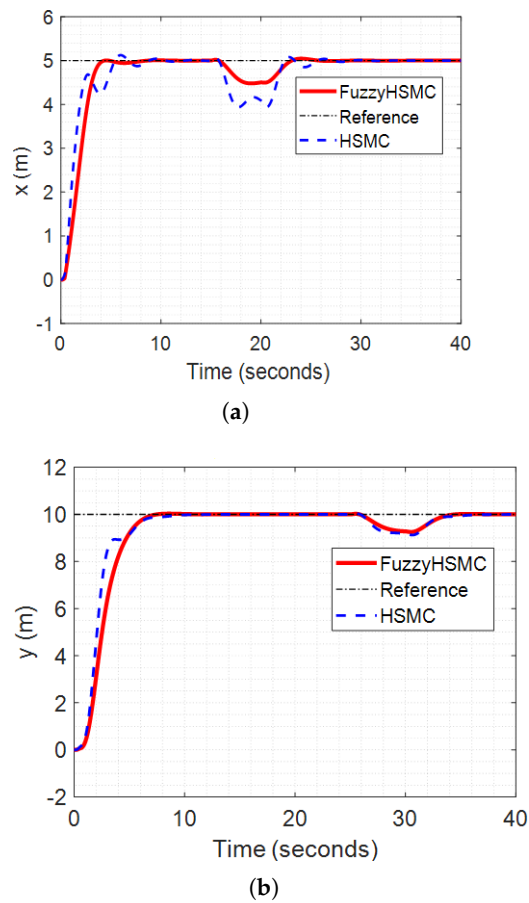
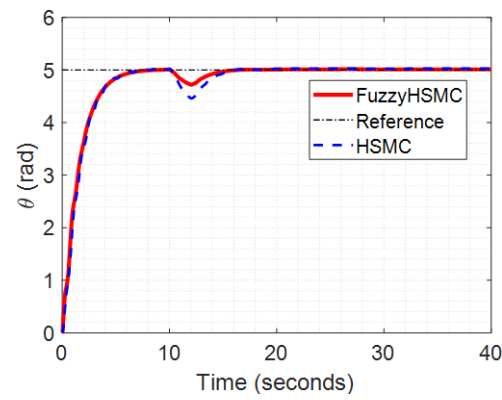
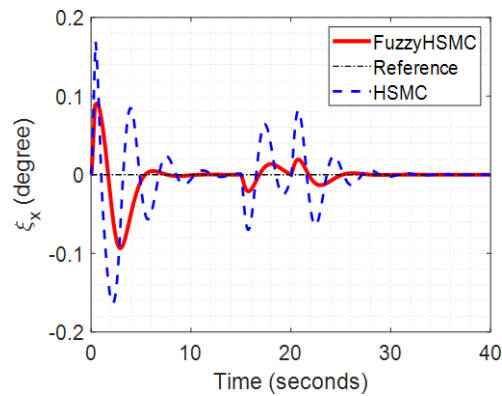


**Figure 9.** Cont.

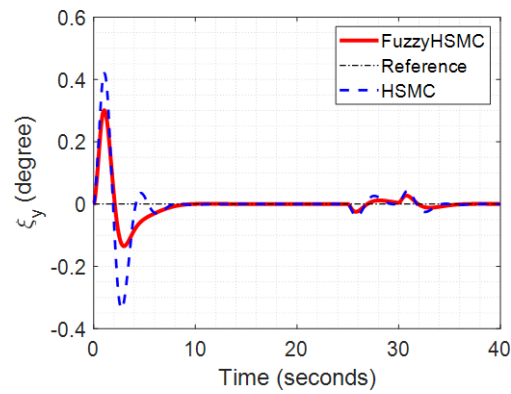


(c)

**Figure 9.** The actuated states under the external disturbances. (a) The trolley position  $x(t)$ . (b) The bridge position  $y(t)$ . (c) The pulley angle  $\theta(t)$ .



(a)



(b)

**Figure 10.** Cont.

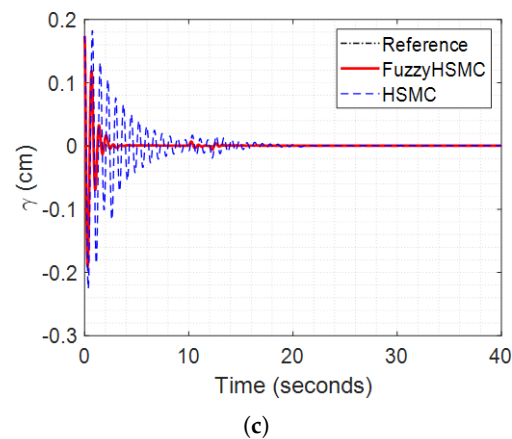


**Figure 10.** The under-actuated states under the external disturbances. (a) The sway of the payload in  $Oxz$ ,  $\xi_x(t)$ . (b) The sway of the payload in  $Oyz$ ,  $\xi_y(t)$ . (c) The oscillation of the hoisting cable in the cable direction,  $\gamma(t)$ .

## 6. Conclusions

A 3D overhead crane with 6 DoF has been considered in this paper, where the elasticity of its hoisting cable is taken into account. Oscillation caused by the cable elasticity constitutes the 6th under-actuated output in the crane system. In order to design a controller to effectively control the 6 DoF overhead crane, the HSMC technique is exploited. Moreover, the parameters of the HSMC scheme are proposed to be adaptively learned by utilizing the fuzzy inference rule mechanism, where the proposed controller is then called FuzzyHSMC. More importantly, the stability of the crane controlled by the proposed algorithm is theoretically proved by the use of the Lyapunov function, which guarantees the effectiveness of the proposed method. Then, the algorithm was extensively evaluated, where the obtained results are highly promising.

One limitation of the work is that the proposed method has not been verified in a physical system. In future work, we will implement the algorithm in an actual gantry crane.

**Author Contributions:** All the authors discussed the idea, conducted the theoretical research, and formulated the problem. H.V.P., Q.-D.H., D.H. and M.V.P. conducted the implementation of the research. D.M.D., N.H.P., H.X.L., L.N. and T.D.K. researched adaptability and proved stability. H.V.P. and Q.-D.H. wrote the first draft. Then, L.N. edited the manuscript. All authors have read and agreed to the published version of the manuscript.

**Funding:** This work was supported and funded by the Hanoi University of Industry under Grant number 14 -2021-RD/HD-DHCN.

**Conflicts of Interest:** The authors declare no conflict of interest.

## Appendix A

The coefficients of the matrix  $M(\chi, t)$  are computed as follows.

$$m_{11} = m_c + m_t.$$

$$m_{21} = 0.$$

$$m_{12} = m_{21}.$$

$$m_{31} = m_c r \sin(\xi_x(t)), m_{13} = m_{31}.$$

$$m_{14} = m_c(\gamma(t) + \Delta\gamma + r(\theta(t) + \xi_x(t)))\cos(\xi_x(t)).$$

$$m_{14} = m_{41}.$$

$$m_{51} = m_{15} = 0.$$

$$m_{61} = m_{16} = m_c \sin(\xi_x(t)).$$

$$m_{22} = m_c + m_b + m_t.$$

$$m_{32} = m_{23} = m_c r \cos(\xi_x(t)) \sin(\xi_y(t)).$$

$$\begin{aligned}
 m_{42} = m_{24} &= \left\{ \begin{array}{l} m_c r \cos(\xi_x(t)) \sin(\xi_y(t)) - \\ -m_c \gamma(t) \sin(\xi_x(t)) \sin(\xi_y(t)) - \\ -m_c r \theta(t) \sin(\xi_x(t)) \sin(\xi_y(t)) - \\ -m_c \Delta \gamma \sin(\xi_x(t)) \sin(\xi_y(t)) - \\ -m_c r \xi_x(t) \sin(\xi_x(t)) \sin(\xi_y(t)) \end{array} \right\}. \\
 m_{52} = m_{25} &= m_c \left\{ \begin{array}{l} \gamma(t) + \Delta \gamma + \\ +r(\theta(t) + \xi_x(t)) \end{array} \right\} \cos(\xi_x(t)) \cos(\xi_y(t)). \\
 m_{62} = m_{26} &= m_c \cos(\xi_x(t)) \sin(\xi_y(t)). \\
 m_{33} &= \left\{ \begin{array}{l} J + m_c r^2 \cos^2(\xi_x(t)) \cos^2(\xi_y(t)) + \\ +m_c r^2 \cos^2(\xi_x(t)) \sin^2(\xi_y(t)) + \\ +m_c r^2 \sin^2(\xi_x(t)) \end{array} \right\}. \\
 m_{43} = m_{34} &= \left\{ \begin{array}{l} m_c r (\gamma(t) + \Delta \gamma + r(\theta(t) + \xi_x(t))) \times \\ \cos(\xi_x(t)) \sin(\xi_x(t)) \\ -m_c r (\gamma(t) + \Delta \gamma + r(\theta(t) + \xi_x(t))) \times \\ \cos^2(\xi_x(t)) \sin^2(\xi_x(t)) \\ -m_c r^2 \cos^2(\xi_x(t)) \sin^2(\xi_y(t)) \end{array} \right\}. \\
 m_{53} = m_{35} &= \frac{1}{4} m_c r^2 \sin(2\xi_x(t)) \sin(2\xi_y(t)). \\
 m_{63} = m_{36} &= m_c r. \\
 m_{44} = m_c &\left\{ \begin{array}{l} -r(\gamma(t) + \Delta \gamma + r(\theta(t) + \xi_x(t))) \times \\ \sin^2(\xi_y(t)) \sin(2\xi_x(t)) + \\ +(\gamma(t) + \Delta \gamma + r(\theta(t) + \xi_x(t)))^2 \times \\ \times \cos^2(\xi_x(t)) + \\ +(\gamma(t) + \Delta \gamma + r(\theta(t) + \xi_x(t)))^2 \times \\ \times \sin^2(\xi_x(t)) \cos^2(\xi_y(t)) + \\ +r^2 \sin^2(\xi_y(t)) \cos^2(\xi_x(t)) + \\ +(\gamma(t) + \Delta \gamma + r(\theta(t) + \xi_x(t)))^2 \times \\ \times \sin^2(\xi_y(t)) \sin^2(\xi_x(t)) \end{array} \right\}. \\
 m_{54} = m_c &\left\{ \begin{array}{l} r(\gamma(t) + \Delta \gamma + r(\theta(t) + \xi_x(t))) \times \\ \times \sin^2(\xi_y(t)) \sin(2\xi_x(t)) + \\ +(\gamma(t) + \Delta \gamma + r(\theta(t) + \xi_x(t)))^2 \times \\ \times \cos^2(\xi_x(t)) + \\ +(\gamma(t) + \Delta \gamma + r(\theta(t) + \xi_x(t)))^2 \times \\ \times \sin^2(\xi_x(t)) \cos^2(\xi_y(t)) + \\ +(\gamma(t) + \Delta \gamma + r(\theta(t) + \xi_x(t)))^2 \times \\ \times \sin^2(\xi_y(t)) \sin^2(\xi_x(t)) + \\ +r^2 \sin^2(\xi_y(t)) \cos^2(\xi_x(t)) \end{array} \right\}. \\
 m_{45} = m_{54}. \\
 m_{64} = m_{46} &= m_c \times \left\{ \begin{array}{l} r \theta(t) \sin^2(\xi_y(t)) \cos(\xi_x(t)) \sin(\xi_x(t)) + \\ +r \xi_x(t) \sin^2(\xi_y(t)) \cos(\xi_x(t)) \sin(\xi_x(t)) + \\ +\gamma(t) \sin^2(\xi_y(t)) \cos(\xi_x(t)) \sin(\xi_x(t)) + \\ +\Delta \gamma \sin^2(\xi_y(t)) \cos(\xi_x(t)) \sin(\xi_x(t)) + \\ +r \sin^2(\xi_y(t)) \cos^2(\xi_x(t)) - \\ -r(\theta(t) + \xi_x(t)) \sin^2(\xi_y(t)) \cos(\xi_x(t)) \times \\ \times \sin(\xi_x(t)) - \\ -\gamma(t) \sin^2(\xi_y(t)) \cos(\xi_x(t)) \sin(\xi_x(t)) - \\ -\Delta \gamma \sin^2(\xi_y(t)) \cos(\xi_x(t)) \sin(\xi_x(t)) \end{array} \right\}.
 \end{aligned}$$

$$m_{55} = m_c \times \left\{ \begin{array}{l} \gamma^2(t)\cos^2(\xi_x(t)) + r^2\theta^2(t)\cos^2(\xi_x(t)) + \\ +\gamma^2(t)\cos^2(\xi_x(t)) + r^2\dot{\xi}_x^2(t)\cos^2(\xi_x(t)) + \\ +2\gamma(t)\Delta\gamma\cos^2(\xi_x(t)) + \\ +2r\gamma(t)\theta(t)\cos^2(\xi_x(t)) + \\ +2r\gamma(t)\dot{\xi}_x(t)\cos^2(\xi_x(t)) + \\ +2\Delta\gamma r\theta(t)\cos^2(\xi_x(t)) + \\ +2r^2\dot{\xi}_x(t)\theta(t)\cos^2(\xi_x(t)) + \\ +2\Delta\gamma r\dot{\xi}_x(t)\cos^2(\xi_x(t)) + \\ +r^2\sin^2(\xi_x(t))\sin^2(\xi_y(t)) - \\ -r\gamma(t)\sin^2(\xi_y(t))\sin(2\xi_x(t)) - \\ -r(\Delta\gamma + r\theta(t) + r\dot{\xi}_x(t))\sin^2(\xi_y(t)) \times \\ \times \sin(2\xi_x(t)) \end{array} \right\}.$$

$$m_{65} = m_{56} = m_c r \cos(\xi_x(t)) \cos(\xi_y(t)) \sin(\xi_x(t)) \sin(\xi_y(t)).$$

$$m_{66} = m_c.$$

Likewise, the coefficients of matrix  $C(\chi, \dot{\chi}, t)$  are calculated by

$$c_{11} = c_{21} = c_{31} = c_{41} = c_{51} = c_{61} = 0.$$

$$c_{12} = c_{22} = c_{32} = c_{42} = c_{52} = c_{62} = 0.$$

$$c_{13} = 2m_c r \dot{\xi}_x(t) \cos(\xi_x(t)).$$

$$c_{14} = m_c \left\{ \begin{array}{l} r\dot{\xi}_x(t) \cos(\xi_x(t)) - \\ -\gamma(t)\dot{\xi}_x(t) \sin(\xi_x(t)) - \\ -\Delta\gamma\dot{\xi}_x(t) \sin(\xi_x(t)) - \\ -r\theta(t)\dot{\xi}_x(t) \sin(\xi_x(t)) - \\ -r\dot{\xi}_x(t)\dot{\xi}_x(t) \sin(\xi_x(t)) \end{array} \right\}.$$

$$c_{15} = 0, c_{16} = 2m_c \dot{\xi}_x(t) \cos(\xi_x(t)).$$

$$c_{23} = 2m_c r \left\{ \begin{array}{l} \dot{\xi}_y(t) \cos(\xi_x(t)) \cos(\xi_y(t)) - \\ -\dot{\xi}_x(t) \sin(\xi_x(t)) \sin(\xi_y(t)) \end{array} \right\}.$$

$$c_{24} = m_c \left\{ \begin{array}{l} 2r\dot{\xi}_y(t) \cos(\xi_x(t)) \cos(\xi_y(t)) - \\ -r\dot{\xi}_x(t)\dot{\xi}_x(t) \cos(\xi_x(t)) \sin(\xi_y(t)) - \\ -\gamma(t)\dot{\xi}_x(t) \cos(\xi_x(t)) \sin(\xi_y(t)) - \\ -r\theta(t)\dot{\xi}_x(t) \cos(\xi_x(t)) \sin(\xi_y(t)) - \\ -\Delta\gamma\dot{\xi}_x(t) \cos(\xi_x(t)) \sin(\xi_y(t)) - \\ -2r\dot{\xi}_x(t) \sin(\xi_x(t)) \sin(\xi_y(t)) \end{array} \right\}.$$

$$c_{25} = -m_c \left\{ \begin{array}{l} 2\dot{\xi}_x(t) \sin(\xi_x(t)) \cos(\xi_y(t)) \times \\ \times (\gamma(t) + \Delta\gamma) + \\ +2r\dot{\xi}_x(t) \sin(\xi_x(t)) \cos(\xi_y(t)) \times \\ \times (\xi_x(t) + \theta(t)) + \dot{\xi}_y(t) \cos(\xi_x(t)) \times \\ \times \sin(\xi_y(t)) (\gamma(t) + \Delta\gamma) + \\ +r\dot{\xi}_y(t) \cos(\xi_x(t)) \times \\ \times \sin(\xi_y(t)) ((\xi_x(t) + \theta(t))) \end{array} \right\}.$$

$$c_{26} = 2m_c \left\{ \begin{array}{l} \dot{\xi}_y(t) \cos(\xi_x(t)) \cos(\xi_y(t)) - \\ -\dot{\xi}_x(t) \sin(\xi_x(t)) \sin(\xi_y(t)) \end{array} \right\}.$$

$$c_{33} = 0.$$

$$c_{34} = m_c r \left\{ \begin{aligned} & -(\dot{\zeta}_x(t) \cos^2(\zeta_x(t)) \cos^2(\zeta_y(t))) \times \\ & \times (\gamma(t) + \Delta\gamma) - \\ & -r(\dot{\zeta}_x(t) \cos^2(\zeta_x(t)) \cos^2(\zeta_y(t))) \times \\ & \times (\zeta_x(t) + \theta(t)) - \\ & -r\dot{\zeta}_x(t) \sin(\zeta_x(t)) \cos(\zeta_x(t)) \times \\ & \times \cos^2(\zeta_y(t)) + 2r \cos^2(\zeta_x(t)) \times \\ & \times \sin(\zeta_y(t)) \dot{\zeta}_y(t) \cos(\zeta_y(t)) - \\ & -2r\dot{\zeta}_x(t) \cos(\zeta_x(t)) \sin^2(\zeta_y(t)) \times \\ & \times \sin(\zeta_x(t)) + \dot{\zeta}_x(t) \cos^2(\zeta_x(t)) \times \\ & \times \sin^2(\zeta_y(t)) (\gamma(t) + \Delta\gamma) + \\ & + r\dot{\zeta}_x(t) \cos^2(\zeta_x(t)) \sin^2(\zeta_y(t)) \times \\ & \times (\zeta_x(t) + \theta(t)) + \\ & + r\dot{\zeta}_x(t) \cos(\zeta_x(t)) \sin(\zeta_x(t)) - \\ & -\dot{\zeta}_x(t) \sin^2(\zeta_x(t)) (\gamma(t) + r\theta(t)) - \\ & -\dot{\zeta}_x(t) \sin^2(\zeta_x(t)) (\Delta\gamma + r\dot{\zeta}_x(t)) + \\ & + \frac{1}{2} \dot{\zeta}_y(t) \sin(2\zeta_x(t)) \sin(2\zeta_y(t)) \times \\ & \times (\gamma(t) + \Delta\gamma) + \frac{1}{2} r \dot{\zeta}_y(t) \times \\ & \times \sin(2\zeta_x(t)) \sin(2\zeta_y(t)) (\zeta_x(t) + \theta(t)) \end{aligned} \right\}.$$

$$c_{35} = m_c r \left\{ \begin{aligned} & r\dot{\zeta}_y(t) \sin(\zeta_x(t)) \cos(\zeta_x(t)) \times \\ & \times \cos^2(\zeta_y(t)) - \dot{\zeta}_y(t) \cos^2(\zeta_x(t)) \times \\ & \times \cos^2(\zeta_y(t)) (\gamma(t) + \Delta\gamma) - \\ & -r\dot{\zeta}_y(t) \cos^2(\zeta_x(t)) \cos^2(\zeta_y(t)) \times \\ & \times (\zeta_x(t) + \theta(t)) - \frac{1}{2} \dot{\zeta}_x(t) \sin(2\zeta_x(t)) \times \\ & \times \sin(2\zeta_y(t)) (\gamma(t) + \Delta\gamma) - \\ & -\frac{1}{2} r \dot{\zeta}_x(t) \sin(2\zeta_x(t)) \sin(2\zeta_y(t)) \times \\ & \times (\zeta_x(t) + \theta(t)) - \\ & -\dot{\zeta}_y(t) \cos^2(\zeta_x(t)) \sin^2 \times \\ & \times (\zeta_y(t)) (\gamma(t) + \Delta\gamma) - \\ & -r\dot{\zeta}_y(t) \cos^2(\zeta_x(t)) \sin^2(\zeta_y(t)) \zeta_x(t) - \\ & -r\dot{\zeta}_y(t) \cos^2(\zeta_x(t)) \sin^2(\zeta_y(t)) \theta(t) \end{aligned} \right\}.$$

$c_{36} = 0.$

$$c_{43} = 2m_c r \left\{ \begin{aligned} & \dot{\zeta}_x(t) (\gamma(t) + \Delta\gamma + r\dot{\zeta}_x(t) + r\theta(t)) + \\ & + r\dot{\zeta}_y(t) \cos^2(\zeta_x(t)) \cos(\zeta_y(t)) \times \\ & \times \sin(\zeta_y(t)) - r\dot{\zeta}_x(t) \cos(\zeta_x(t)) \times \\ & \times \sin(\zeta_x(t)) \sin^2(\zeta_y(t)) \end{aligned} \right\}.$$

$$\begin{aligned}
 c_{44} = m_c \times & \left\{ \begin{aligned} & - \left\{ \begin{aligned} & \sin(\zeta_x(t)) \sin(\zeta_y(t)) (\gamma(t) + \Delta\gamma) + \\ & + r \sin(\zeta_x(t)) \sin(\zeta_y(t)) \times \\ & \times (\zeta_x(t) + \theta(t)) - \\ & - r \cos(\zeta_x(t)) \sin(\zeta_y(t)) \end{aligned} \right\} \times \\ & \times \left\{ \begin{aligned} & 2r\dot{\zeta}_y(t) \cos(\zeta_x(t)) \cos(\zeta_y(t)) - \\ & - 2r\dot{\zeta}_x(t) \sin(\zeta_x(t)) \sin(\zeta_y(t)) - \\ & - \dot{\zeta}_x(t) \cos(\zeta_x(t)) \sin(\zeta_y(t)) \times \\ & \times (\gamma(t) + \Delta\gamma) - \\ & - r\dot{\zeta}_x(t) \cos(\zeta_x(t)) \sin(\zeta_y(t)) \times \\ & \times (\zeta_x(t) + \theta(t)) \end{aligned} \right\} + \\ & + \cos(\zeta_x(t)) \cos(\zeta_y(t)) \times \\ & \times (\gamma(t) + \Delta\gamma + r\zeta_x(t) + r\theta(t)) \times \\ & \times \left\{ \begin{aligned} & \dot{\zeta}_x(t) \cos(\zeta_x(t)) \cos(\zeta_y(t)) \times \\ & \times (\gamma(t) + \Delta\gamma) + \\ & + r\dot{\zeta}_x(t) \cos(\zeta_x(t)) \cos(\zeta_y(t)) \times \\ & \times (\zeta_x(t) + \theta(t)) - \\ & - 2\dot{\zeta}_y(t) \sin(\zeta_x(t)) \sin(\zeta_y(t)) \times \\ & \times (\gamma(t) + \Delta\gamma) - \\ & - 2r\dot{\zeta}_y(t) \sin(\zeta_x(t)) \sin(\zeta_y(t)) \times \\ & \times (\zeta_x(t) + \theta(t)) - \\ & - r\dot{\zeta}_x(t) \sin(\zeta_x(t)) \cos(\zeta_y(t)) \end{aligned} \right\} + \\ & + \left\{ \begin{aligned} & r\dot{\zeta}_x(t) \cos^2(\zeta_x(t)) \\ & - \dot{\zeta}_x(t) \sin(\zeta_x(t)) (\gamma(t) + r\zeta_x(t)) \\ & - \dot{\zeta}_x(t) \sin(\zeta_x(t)) (\Delta\gamma + r\theta(t)) \end{aligned} \right\} \times \\ & \times \left\{ \begin{aligned} & \gamma(t) + r\zeta_x(t) \\ & + \Delta\gamma + r\theta(t) \end{aligned} \right\} \end{aligned} \right\} \\
 c_{45} = m_c \times & \left\{ \begin{aligned} & \left\{ \begin{aligned} & \sin(\zeta_x(t)) \sin(\zeta_y(t)) (\gamma(t) + \Delta\gamma) + \\ & + r \sin(\zeta_x(t)) \sin(\zeta_y(t)) \theta(t) + \\ & + r \sin(\zeta_x(t)) \sin(\zeta_y(t)) \zeta_x(t) - \\ & - r \cos(\zeta_x(t)) \sin(\zeta_y(t)) \end{aligned} \right\} \times \\ & \times \left\{ \begin{aligned} & 2\dot{\zeta}_x(t) \sin(\zeta_x(t)) \cos(\zeta_y(t)) + \\ & + \dot{\zeta}_y(t) \cos(\zeta_x(t)) \sin(\zeta_y(t)) \end{aligned} \right\} \times \\ & \times \left\{ \begin{aligned} & \gamma(t) + r\zeta_x(t) + \\ & + \Delta\gamma + r\theta(t) \end{aligned} \right\} - \\ & - \left\{ \begin{aligned} & r\dot{\zeta}_y(t) \sin(\zeta_x(t)) \cos(\zeta_y(t)) - \\ & - \dot{\zeta}_y(t) \cos(\zeta_x(t)) \cos(\zeta_y(t)) \times \\ & \times (\gamma(t) + r\zeta_x(t)) - \\ & - \dot{\zeta}_y(t) \cos(\zeta_x(t)) \cos(\zeta_y(t)) \times \\ & \times (\Delta\gamma + r\theta(t)) \end{aligned} \right\} \times \\ & \times \sin(\zeta_x(t)) \cos(\zeta_y(t)) \times \\ & \times (\gamma(t) + \Delta\gamma + r\zeta_x(t) + r\theta(t)) \end{aligned} \right\} \\
 c_{46} = 2m_c & \left\{ \begin{aligned} & \dot{\zeta}_x(t) (\gamma(t) + \Delta\gamma + r\zeta_x(t) + r\theta(t)) + \\ & + r\dot{\zeta}_y(t) \cos^2(\zeta_x(t)) \cos(\zeta_y(t)) \times \\ & \times \sin(\zeta_y(t)) - r\dot{\zeta}_x(t) \cos(\zeta_x(t)) \times \\ & \times \sin(\zeta_x(t)) \sin^2(\zeta_y(t)) \end{aligned} \right\} \\
 c_{53} = 2m_c r & \left\{ \begin{aligned} & \dot{\zeta}_y(t) \cos^2(\zeta_x(t)) \times \\ & \times (\gamma(t) + \Delta\gamma + r\zeta_x(t) + r\theta(t)) - \\ & - r\dot{\zeta}_x(t) \sin^2(\zeta_x(t)) \cos(\zeta_y(t)) \times \\ & \times \sin(\zeta_y(t)) - r\dot{\zeta}_y(t) \cos(\zeta_x(t)) \times \\ & \times \sin(\zeta_x(t)) \sin^2(\zeta_y(t)) \end{aligned} \right\}
 \end{aligned}$$

$$\begin{aligned}
 c_{54} &= m_c \times \left\{ \begin{aligned} &\cos(\zeta_x(t)) \cos(\zeta_y(t)) \times \\ &\times (\gamma(t) + \Delta\gamma + r\dot{\zeta}_x(t) + r\theta(t)) \times \\ &\times \left\{ \begin{aligned} &2r \left\{ \begin{aligned} &\dot{\zeta}_y(t) \cos(\zeta_x(t)) \cos(\zeta_y(t)) - \\ &-\dot{\zeta}_x(t) \sin(\zeta_x(t)) \sin(\zeta_y(t)) \end{aligned} \right\} \\ &-\dot{\zeta}_x(t) \cos(\zeta_x(t)) \sin(\zeta_y(t)) \times \\ &\times (\gamma(t) + \Delta\gamma) - \\ &-r\dot{\zeta}_x(t) \cos(\zeta_x(t)) \sin(\zeta_y(t)) \zeta_x(t) - \\ &-r\dot{\zeta}_x(t) \cos(\zeta_x(t)) \sin(\zeta_y(t)) \theta(t) \end{aligned} \right\} - \\ &\left\{ \begin{aligned} &r \sin(\zeta_x(t)) \sin(\zeta_y(t)) - \\ &-\cos(\zeta_x(t)) \sin(\zeta_y(t)) (\gamma(t) + \Delta\gamma) - \\ &-r \cos(\zeta_x(t)) \sin(\zeta_y(t)) \zeta_x(t) - \\ &-r \cos(\zeta_x(t)) \sin(\zeta_y(t)) \theta(t) \end{aligned} \right\} \times \end{aligned} \right\} \\
 c_{55} &= m_c \times \left\{ \begin{aligned} &\left\{ \begin{aligned} &\dot{\zeta}_x(t) \cos(\zeta_x(t)) \cos(\zeta_y(t)) \times \\ &\times (\gamma(t) + r\dot{\zeta}_x(t) + \dot{\zeta}_x(t) \cos(\zeta_x(t)) \times \\ &\times \cos(\zeta_y(t)) (\Delta\gamma + r\theta(t)) - 2\dot{\zeta}_y(t) \times \\ &\times \sin(\zeta_x(t)) \sin(\zeta_y(t)) \times \\ &\times (\gamma(t) + r\dot{\zeta}_x(t) - 2\dot{\zeta}_y(t) \sin(\zeta_x(t)) \times \\ &\times \sin(\zeta_y(t)) (\Delta\gamma + r\theta(t)) + \\ &+r\dot{\zeta}_x(t) \sin(\zeta_x(t)) \cos(\zeta_y(t)) \end{aligned} \right\} \\ &\left\{ \begin{aligned} &r\dot{\zeta}_y(t) \sin(\zeta_x(t)) \cos(\zeta_y(t)) - \\ &-\dot{\zeta}_y(t) \cos(\zeta_x(t)) \cos(\zeta_y(t)) \gamma(t) - \\ &-r\dot{\zeta}_y(t) \cos(\zeta_x(t)) \cos(\zeta_y(t)) \zeta_x(t) - \\ &-r\dot{\zeta}_y(t) \cos(\zeta_x(t)) \cos(\zeta_y(t)) \theta(t) - \\ &-\dot{\zeta}_y(t) \cos(\zeta_x(t)) \cos(\zeta_y(t)) \Delta\gamma \end{aligned} \right\} \times \\ &\times \left\{ \begin{aligned} &r \sin(\zeta_x(t)) \sin(\zeta_y(t)) - \\ &-\cos(\zeta_x(t)) \sin(\zeta_y(t)) \times \\ &\times (\gamma(t) + r\dot{\zeta}_x(t)) - \\ &-\cos(\zeta_x(t)) \sin(\zeta_y(t)) \times \\ &\times (\Delta\gamma + r\theta(t)) \end{aligned} \right\} - \\ &-\cos(\zeta_x(t)) \cos(\zeta_y(t)) \left\{ \begin{aligned} &\gamma(t) + \Delta\gamma \\ &+r\dot{\zeta}_x(t) + r\theta(t) \end{aligned} \right\}^2 \times \\ &\times \left\{ \begin{aligned} &2\dot{\zeta}_x(t) \sin(\zeta_x(t)) \cos(\zeta_y(t)) + \\ &+\dot{\zeta}_y(t) \cos(\zeta_x(t)) \sin(\zeta_y(t)) \end{aligned} \right\} \end{aligned} \right\} \\
 c_{56} &= 2m_c \times \left\{ \begin{aligned} &\dot{\zeta}_y(t) \cos^2(\zeta_x(t)) \times \\ &\times (\gamma(t) + \Delta\gamma + r\dot{\zeta}_x(t) + r\theta(t)) - \\ &-r\dot{\zeta}_x(t) \sin^2(\zeta_x(t)) \cos(\zeta_y(t)) \sin(\zeta_y(t)) - \\ &-r\dot{\zeta}_y(t) \cos(\zeta_x(t)) \sin(\zeta_x(t)) \sin^2(\zeta_y(t)) \end{aligned} \right\} \\
 c_{63} &= 0, c_{66} = 0.
 \end{aligned}$$

$$\begin{aligned}
 c_{64} &= m_c \times \left\{ \begin{aligned} &r \sin(\zeta_x(t)) \dot{\zeta}_x(t) \cos(\zeta_x(t)) - \\ &-\sin^2(\zeta_x(t)) \dot{\zeta}_x(t) (\gamma(t) + r\dot{\zeta}_x(t)) - \\ &-\sin^2(\zeta_x(t)) \dot{\zeta}_x(t) (\Delta\gamma + r\theta(t)) - \\ &-\left\{ \begin{aligned} &\cos(\zeta_x(t)) \cos(\zeta_y(t)) \times \\ &\times (\gamma(t) + r\dot{\zeta}_x(t)) + \\ &+ \cos(\zeta_x(t)) \cos(\zeta_y(t)) \times \\ &\times (\Delta\gamma + r\theta(t)) \end{aligned} \right\} \times \\ &\times \left\{ \begin{aligned} &\dot{\zeta}_x(t) \cos(\zeta_x(t)) \cos(\zeta_y(t)) - \\ &-2\dot{\zeta}_y(t) \sin(\zeta_x(t)) \sin(\zeta_y(t)) \end{aligned} \right\} - \\ &-r\dot{\zeta}_x(t) \cos(\zeta_x(t)) \sin(\zeta_x(t)) \cos^2(\zeta_y(t)) + \\ &+2r\dot{\zeta}_y(t) \cos^2(\zeta_x(t)) \cos(\zeta_y(t)) \sin(\zeta_y(t)) - \\ &-2r\dot{\zeta}_x(t) \cos(\zeta_x(t)) \sin(\zeta_x(t)) \sin^2(\zeta_y(t)) - \\ &-\dot{\zeta}_x(t) \cos^2(\zeta_x(t)) \sin^2(\zeta_y(t)) \times \\ &\times (\gamma(t) + r\dot{\zeta}_x(t)) - \\ &-\dot{\zeta}_x(t) \cos^2(\zeta_x(t)) \sin^2(\zeta_y(t)) (\Delta\gamma + r\theta(t)) \end{aligned} \right\}. \\
 c_{65} &= m_c \times \left\{ \begin{aligned} &-\frac{1}{2}\dot{\zeta}_x(t) \sin(2\zeta_x(t)) \sin(2\zeta_y(t)) \gamma(t) - \\ &-\frac{1}{2}r\dot{\zeta}_x(t) \sin(2\zeta_x(t)) \sin(2\zeta_y(t)) \dot{\zeta}_x(t) - \\ &-\frac{1}{2}r\dot{\zeta}_x(t) \sin(2\zeta_x(t)) \sin(2\zeta_y(t)) \theta(t) - \\ &-\dot{\zeta}_y(t) \cos^2(\zeta_x(t)) \sin^2(\zeta_y(t)) \times \\ &\times (\gamma(t) + r\dot{\zeta}_x(t)) - \\ &-\dot{\zeta}_y(t) \cos^2(\zeta_x(t)) \sin^2(\zeta_y(t)) (\Delta\gamma + r\theta(t)) + \\ &+r\dot{\zeta}_y(t) \cos(\zeta_x(t)) \sin(\zeta_y(t)) \cos^2(\zeta_y(t)) - \\ &-\dot{\zeta}_y(t) \cos^2(\zeta_x(t)) \cos^2(\zeta_y(t)) (\gamma(t) + \Delta\gamma) - \\ &-r\dot{\zeta}_y(t) \cos^2(\zeta_x(t)) \cos^2(\zeta_y(t)) \dot{\zeta}_x(t) - \\ &-r\dot{\zeta}_y(t) \cos^2(\zeta_x(t)) \cos^2(\zeta_y(t)) \theta(t) - \\ &-\frac{1}{2}\dot{\zeta}_x(t) \sin(2\zeta_x(t)) \sin(2\zeta_y(t)) \Delta\gamma \end{aligned} \right\}.
 \end{aligned}$$

And, the coefficients of vector  $G(\chi, t)$  are computed by

$$g_1 = m_c g r \cos(\zeta_x(t)) \cos(\zeta_y(t)).$$

$$g_2 = - \left\{ \begin{aligned} &m_c g \gamma(t) \sin(\zeta_x(t)) \cos(\zeta_y(t)) + \\ &+m_c g \Delta\gamma \sin(\zeta_x(t)) \cos(\zeta_y(t)) + \\ &+m_c g r \theta(t) \sin(\zeta_x(t)) \cos(\zeta_y(t)) + \\ &+m_c g r \dot{\zeta}_x(t) \sin(\zeta_x(t)) \cos(\zeta_y(t)) \end{aligned} \right\}.$$

$$g_3 = - \left\{ \begin{aligned} &m_c g \gamma(t) \sin(\zeta_y(t)) \cos(\zeta_x(t)) + \\ &+m_c g \Delta\gamma \sin(\zeta_y(t)) \cos(\zeta_x(t)) + \\ &+m_c g r \theta(t) \sin(\zeta_y(t)) \cos(\zeta_x(t)) + \\ &+m_c g r \dot{\zeta}_x(t) \sin(\zeta_y(t)) \cos(\zeta_x(t)) - \\ &-m_c g r \sin(\zeta_x(t)) \sin(\zeta_y(t)) \end{aligned} \right\}.$$

$$g_4 = m_c g \cos(\zeta_x(t)) \cos(\zeta_y(t)) + \rho \Delta\gamma.$$

**References**

1. Van Nguyen, T.; Le, H.X.; Tran, H.V.; Nguyen, D.A.; Nguyen, M.N.; Nguyen, L. An Efficient Approach for SIMO Systems using Adaptive Fuzzy Hierarchical Sliding Mode Control. In Proceedings of the 2021 IEEE International Conference on Autonomous Robot Systems and Competitions (ICARSC), Santa Maria da Feira, Portugal, 28–29 April 2021; pp. 85–90. [\[CrossRef\]](#)
2. Li, Y.; Xi, X.; Xie, J.; Liu, C. Study and Implementation of a Cooperative Hoisting for Two Crawler Cranes. *J. Intell. Robot. Syst.* **2016**, *83*, 165–178. [\[CrossRef\]](#)
3. Xing, X.; Liu, J. Vibration and Position Control of Overhead Crane with Three-Dimensional Variable Length Cable Subject to Input Amplitude and Rate Constraints. *IEEE Trans. Syst. Man Cybern. Syst.* **2021**, *51*, 4127–4138. [\[CrossRef\]](#)
4. Campeau-Lecours, A.; Foucault, S.; Laliberté, T.; Mayer-St-Onge, B.; Gosselin, C. A Cable-Suspended Intelligent Crane Assist Device for the Intuitive Manipulation of Large Payloads. *IEEE/ASME Trans. Mechatron.* **2016**, *21*, 2073–2084. [\[CrossRef\]](#)
5. Rigatos, G.; Siano, P.; Abbaszadeh, M. Nonlinear H-infinity control for 4-DOF underactuated overhead cranes. *Trans. Inst. Meas. Control* **2018**, *40*, 2364–2377. [\[CrossRef\]](#)
6. Mahapatra, S.; Subudhi, B. Design and experimental realization of a backstepping nonlinear H $\infty$  control for an autonomous underwater vehicle using a nonlinear matrix inequality approach. *Trans. Inst. Meas. Control* **2018**, *40*, 3390–3403. [\[CrossRef\]](#)

7. Le, H.X.; Nguyen, L.; Thiyagarajan, K. A Dynamic Surface Controller based on Adaptive Neural Network for Dual Arm Robots. In Proceedings of the 2020 15th IEEE Conference on Industrial Electronics and Applications (ICIEA), Kristiansand, Norway, 9–13 November 2020; pp. 555–560.
8. Nguyen, T.V.; Thai, N.H.; Pham, H.T.; Phan, T.A.; Nguyen, L.; Le, H.X.; Nguyen, H.D. Adaptive Neural Network-Based Backstepping Sliding Mode Control Approach for Dual-Arm Robots. *J. Control Autom. Electr. Syst.* **2019**, *30*, 512–521. [[CrossRef](#)]
9. Vu, Q.V.; Dinh, T.A.; Nguyen, T.V.; Tran, H.V.; Le, H.X.; Pham, H.V.; Kim, T.D.; Nguyen, L. An Adaptive Hierarchical Sliding Mode Controller for Autonomous Underwater Vehicles. *Electronics* **2021**, *10*, 2316. [[CrossRef](#)]
10. Pham, D.T.; Nguyen, T.V.; Le, H.X.; Nguyen, L.; Thai, N.H.; Phan, T.A.; Pham, H.T.; Duong, A.H.; Bui, L.T. Adaptive neural network based dynamic surface control for uncertain dual arm robots. *Int. J. Dyn. Control* **2020**, *8*, 824–834. [[CrossRef](#)]
11. Hoang, U.T.T.; Le, H.X.; Thai, N.H.; Pham, H.V.; Nguyen, L. Consistency of Control Performance in 3D Overhead Cranes under Payload Mass Uncertainty. *Electronics* **2020**, *9*, 657. [[CrossRef](#)]
12. Le, V.A.; Le, H.X.; Nguyen, L.; Phan, M.X. An Efficient Adaptive Hierarchical Sliding Mode Control Strategy Using Neural Networks for 3D Overhead Cranes. *Int. J. Autom. Comput.* **2019**, *16*, 614–627. [[CrossRef](#)]
13. Le, H.X.; Le, A.V.; Nguyen, L. Adaptive fuzzy observer based hierarchical sliding mode control for uncertain 2D overhead cranes. *Cyber-Phys. Syst.* **2019**, *5*, 191–208. [[CrossRef](#)]
14. Fu, Y.; Sun, N.; Yang, T.; Qiu, Z.; Fang, Y. Adaptive Coupling Anti-Swing Tracking Control of Underactuated Dual Boom Crane Systems. *IEEE Trans. Syst. Man Cybern. Syst.* **2021**, *3*, 1–13. [[CrossRef](#)]
15. Xu, W.; Zheng, X.; Liu, Y.; Zhang, M.; Luo, Y. Adaptive dynamic sliding mode control for overhead cranes. In Proceedings of the 2015 34th Chinese Control Conference (CCC), Hangzhou, China, 28–30 July 2015; pp. 3287–3292.
16. Li, Y.; Zhou, S.; Zhu, H. A backstepping controller design for underactuated crane system. In Proceedings of the 2018 Chinese Control and Decision Conference (CCDC), Shenyang, China, 9–11 June 2018; pp. 2895–2899. [[CrossRef](#)]
17. Tsai, C.C.; Wu, H.L.; Chuang, K.H. Backstepping aggregated sliding-mode motion control for automatic 3D overhead cranes. In Proceedings of the 2012 IEEE/ASME International Conference on Advanced Intelligent Mechatronics (AIM), Kaohsiung, Taiwan, 11–14 July 2012; pp. 849–854. [[CrossRef](#)]
18. Yang, T.; Sun, N.; Fang, Y. Adaptive Fuzzy Control for a Class of MIMO Underactuated Systems with Plant Uncertainties and Actuator Deadzones: Design and Experiments. *IEEE Trans. Cybern.* **2021**, 1–14. [[CrossRef](#)] [[PubMed](#)]
19. Yang, T.; Sun, N.; Fang, Y. Neuroadaptive Control for Complicated Underactuated Systems with Simultaneous Output and Velocity Constraints Exerted on Both Actuated and Unactuated States. *IEEE Trans. Neural Netw. Learn. Syst.* **2021**, 1–11. [[CrossRef](#)] [[PubMed](#)]
20. Wang, W.; Yi, J.; Zhao, D.; Liu, D. Design of a stable sliding-mode controller for a class of second-order underactuated systems. *IEE Proc.-Control Theory Appl.* **2004**, *151*, 683–690. [[CrossRef](#)]
21. Mahjoub, S.; Mnif, F.; Derbel, N. Second-order sliding mode approaches for the control of a class of underactuated systems. *Int. J. Autom. Comput.* **2015**, *12*, 134–141. [[CrossRef](#)]
22. Zadeh, L.A. Is there a need for fuzzy logic? *Inf. Sci.* **2008**, *178*, 2751–2779. [[CrossRef](#)]
23. Yang, T.; Chen, H.; Sun, N.; Fang, Y. Adaptive Neural Network Output Feedback Control of Uncertain Underactuated Systems with Actuated and Unactuated State Constraints. *IEEE Trans. Syst. Man Cybern. Syst.* **2021**, 1–17. [[CrossRef](#)]
24. Yue, M.; An, C.; Du, Y.; Sun, J. Indirect adaptive fuzzy control for a nonholonomic/underactuated wheeled inverted pendulum vehicle based on a data-driven trajectory planner. *Fuzzy Sets Syst.* **2016**, *290*, 158–177. [[CrossRef](#)]
25. Al-saedi, M.I. Enhancing the Feedforward–Feedback Controller for Nonlinear Overhead Crane Using Fuzzy logic controller. *IOP Conf. Ser. Mater. Sci. Eng.* **2020**, *745*, 012074. [[CrossRef](#)]
26. Zdesar, A.; Cerman, O.; Dovzan, D.; Husek, P.; Skrijanc, I. Fuzzy Control of a Helio-Crane. *J. Intell. Robot. Syst.* **2013**, *72*, 497–515. [[CrossRef](#)]
27. Shi, H.; Li, G.; Bai, X.; Huang, J. Research on Nonlinear Control Method of Underactuated Gantry Crane Based on Machine Vision Positioning. *Symmetry* **2019**, *11*, 987. [[CrossRef](#)]